Hypoxic injury triggers maladaptive repair in human kidney organoids

Ana B. Nunez-Nescolarde[1], Mehran Piran[1], Laura Perlaza-Jiménez[2,3], Chris K. Barlow[4], Joel R. Steele[4], Deanna Deveson[2], Han-Chung Lee[4], Julie L. M. Moreau[1], Ralf B. Schittenhelm[4], David J. Nikolic-Paterson[5†], Alexander N. Combes[1†*]

[1]Department of Anatomy and Developmental Biology, Development and Stem Cells Program, Monash Biomedicine Discovery Institute, Monash University; Clayton, Australia.

[2]Monash Bioinformatics Platform, Monash University; Clayton, VIC 3800, Australia

[3]Department of Biochemistry and Molecular Biology, Cancer Program, Monash Biomedicine Discovery Institute, Monash University; Clayton, VIC 3800, Australia

[4]Monash Proteomics and Metabolomics Facility; Monash University, Clayton, VIC 3800, Australia

[5]Department of Nephrology, Monash Health and Monash University Centre for Inflammatory Diseases, Monash Medical Centre; Clayton, VIC 3168, Australia

[†]These authors contributed equally to this work.

*Correspondence: alex.combes@monash.edu

Summary: Human kidney organoids recapitulate molecular and metabolic signatures of ischemic acute kidney injury and maladaptive repair, providing new insight into human disease mechanisms and opportunities for drug development.

ABSTRACT

Acute kidney injury (AKI) is a common clinical disorder linked to high rates of illness and death. Ischemia is a leading cause of AKI, which can result in chronic kidney disease (CKD) through a maladaptive repair process characterised by failed epithelial regeneration, inflammation, and metabolic dysregulation. No targeted therapies exist to prevent the AKI to CKD transition and insight into ischemic AKI and maladaptive repair in humans remains limited. In this study, we report that human kidney organoids recapitulate select molecular and metabolic signatures of AKI and maladaptive repair in response to hypoxic injury. Transcriptional, proteomic, and metabolomic profiling revealed signatures of tubular injury, cell death, cell cycle arrest and altered metabolism in kidney organoids cultured in hypoxic conditions. After recovery in normoxic conditions, injured organoids displayed increased signatures associated with maladaptive repair like TNF, NF-κB, and JAK-STAT pathways, and S100A8/9. Single cell RNA sequencing localised biomarkers of AKI and maladaptive repair such as GDF15, MMP7, ICAM1, TGFB1, SPP1, C3 and CCN1 to injured proximal and distal tubules. Metabolic phenotypes linked to CKD were also evident including dysregulated glycolysis and gluconeogenesis, amino acid, bicarbonate and lipid metabolism, and elevated ceramide levels. Our multi-omic analysis provides compelling evidence for the use of kidney organoids as a model of human ischemic AKI and maladaptive repair, highlighting new and conserved biomarkers and mechanisms, and opportunities for drug screening.

INTRODUCTION

Acute kidney injury (AKI) is a heterogenous and multifactorial syndrome defined by a rapid decline in kidney function. Over 13 million people are estimated to be affected by AKI each year, resulting in 1.7 million related deaths (*1, 2*). Ischemia is a leading cause of AKI, which can arise from many causes including cardiovascular events, urinary tract obstruction, sepsis, and planned interventions like kidney transplantation or cardiopulmonary bypass surgery (*2-4*). Impaired fluid

handling and waste removal during severe AKI can lead to cardiovascular complications, neurotoxicity, organ failure and death. Individuals with mild to moderate AKI can recover renal function in the short term but face a significant risk of developing or exacerbating chronic kidney disease (CKD) and cardiovascular disease. Current management of AKI is limited to treatments to control blood pressure and electrolyte levels, or hemodialysis in severe cases (*2, 3*). However, specific therapies to prevent or intervene in AKI remain an area of unmet clinical need.

Each kidney contains around one million nephrons, which cooperate to filter the blood, regulating fluid and electrolyte balance, acid-base homeostasis, reabsorbing nutrients and eliminating waste. These functions rely on ion gradients and ATP produced by mitochondria to actively transport solutes and fluids across the cell membrane. While the proximal tubule (PT), loop of Henle and distal tubule (DT) all utilise active transport, most solute reabsorption occurs in the PT which has a high mitochondrial content to enable these processes (*5*). Under stressed conditions, mitochondria produce excess reactive oxygen species (ROS) which may explain the susceptibility of the nephron, and especially the PT, to ischemic injury (*5*). During ischemia, reduced blood flow limits the supply of oxygen and nutrients to the kidney causing oxidative stress, endoplasmic reticulum (ER) stress, and inflammation. Low oxygen levels trigger the stabilisation of hypoxia inducible factor 1 subunit alpha (HIF1A), which activates target genes like glycolytic enzyme hexokinase 1 (*HK1*) and angiogenic signal vascular endothelial growth factor A (*VEGFA*) to adapt to and recover from hypoxia (*6*). Despite these adaptations, severe hypoxia can induce tubular cell death through the apoptosis signal-regulating kinase 1/Jun N-terminal kinase (ASK1/JNK), ferroptosis, and necroptosis pathways (*7-10*).

How AKI leads to the development of CKD is a major area of interest for therapeutic intervention. Injured tubules can undergo healthy (adaptive) repair via dedifferentiation and proliferation, mediated in part by SRY-box transcription factor 9 (SOX9) (*11-13*). However, sustained or severe injury can induce maladaptive repair and progression to CKD - a process which is hard to detect after recovery of kidney function post-AKI. Tubules undergoing maladaptive repair express increased levels of injury markers like hepatitis A virus cellular receptor 1 (HAVCR1) and growth differentiation factor 15 (GDF15); as well as inflammatory mediators such intercellular adhesion molecule 1 (ICAM1), vascular cell adhesion molecule 1 (VCAM1), C-C motif chemokine ligand 2 (CCL2), homeo-domain interacting protein kinase 2 (HIPK2), which attract immune cells to the site of injury and activate fibroblast (stromal/myofibroblast) expansion (*14, 15*). Injured PT cells secrete profibrotic factors like transforming growth factor beta 1 (TGFB1) and cellular communication network factor 2 (CCN2, also known as CTGF) that further contribute to fibrosis and CKD (*14, 15*). Metabolic dysregulation is also a feature of maladaptive PT cells, marked by impaired fatty acid oxidation, reduced ATP levels and intracellular lipid accumulation (*16-18*).

Our knowledge of hypoxia-induced AKI and the transition to CKD has largely been derived from rodent models. Validation of these findings in human AKI has been limited to analysis of blood and urine samples since renal biopsy is contraindicated in most AKI settings. While single cell and spatial technologies are beginning to drive insight into rare AKI biopsies (*19*), there remains a need for human experimental models to facilitate mechanistic studies and test new therapeutic strategies. We and others have shown that human induced pluripotent stem cell (iPSC)-derived kidney organoids contain nephron, stromal and endothelial cell types with high congruence to those in the human fetal kidney (*20-22*). Moreover, kidney organoids have demonstrated utility in modelling kidney development, nephrotoxicity, cytokine stressors, and inherited disease (*23-29*). As such, we hypothesised that human kidney organoids may serve to model the tissue-intrinsic mechanisms of ischemic AKI and maladaptive repair.

RESULTS

Hypoxia induces markers of acute injury, proinflammatory and profibrotic signals in human kidney organoids derived from three independent iPSC lines

Kidney organoids were generated from three independent human iPSC lines using the Takasato protocol (*30-32*). Differentiation conditions were optimised for each cell line and the presence of expected human kidney cell types was confirmed (Figure 1A, Supplemental Table 1). Markers of stromal, proximal and distal nephron cell types were expressed by day 18 of differentiation (Supplemental Figure 1), which was used as a starting timepoint for subsequent experiments. Hypoxia has been modelled in proximal tubule cells cultured in 1% oxygen (O_2) for 24-48 h (*33*), whilst most kidney organoid protocols have been established in 19-21% O_2 (*31, 34-37*). As such, kidney organoids were cultured in hypoxic (1% O_2) or 'normoxic' (19% O_2) conditions from days 18-20 and collected at day 20 to asses hypoxic injury, or after a 5-day recovery in normoxic conditions to assess maladaptive repair (Figure 1B). These experimental groups are referred to as follows: day 20 hypoxia (d20h), day 20 normoxic control (d20n), day 25 hypoxic injury/normoxic recovery (d25h/n or 'injured'), day 25 normoxic control (d25n).

Hypoxic AKI is characterized by a HIF1A-mediated response (*38, 39*), followed by tubular injury and cell cycle arrest (*40*). A robust hypoxic response was evident in organoids cultured in 1% O_2 with increased expression of *HIF1A* and target genes vascular endothelial growth factor A (*VEGFA*) and the glycolytic enzyme hexokinase 1 (*HK1*), as measured by quantitative PCR (qPCR) (Figure 1C) (*6, 41*). Master regulator of mitochondrial biogenesis-peroxisome proliferator-activated receptor γ coactivator 1α (*PPARCG1A*), was significantly reduced in d20h kidney organoids, mirroring similar findings in human AKI and IRI, and animal models of sepsis (*42*).

Signs of tubular damage were also evident in d20h organoids with upregulation of the cell cycle arrest marker cyclin dependent kinase inhibitor 1A (*CDKN1A,* also known as p21), and *HAVCR1* (also known as KIM1), and *GDF15*, accompanied by increased *TGFB1* which can drive profibrotic and protective responses after kidney injury (Figure 1C) (*40, 43, 44*). Effective or adaptive repair after AKI can result in a full recovery of kidney function (*45-47*). In contrast, maladaptive repair involves persistent expression of inflammatory cytokines like *CCL2* and increased deposition of extracellular matrix (ECM) components such as collagen type I alpha 1 chain (*COL1A1*) and fibronectin 1 (*FN1*), all of which were significantly increased in d25h/n organoids (Figure 1C). Thus, data from three independent iPSC lines show that human kidney organoids display a robust acute response to hypoxic injury and express select markers associated with maladaptive repair. We next sought to extend analysis of AKI and maladaptive repair signatures using bulk and single-cell transcriptomics, and LC-MS-based proteomics and metabolomics.

Transcriptional profiling identifies markers of AKI and maladaptive repair in organoids cultured under hypoxic conditions

To gain a deeper understanding of the response to hypoxic injury we performed bulk RNA-sequencing (RNA-seq) and differential expression analysis on human kidney organoids from control and hypoxic groups at d20 and d25 (Figure 2A, Supplemental Figure 2A-B, Supplemental File 1). KEGG pathway analysis identified increased signatures related to DNA damage, the hypoxic-response, cell cycle arrest and metabolism in d20 hypoxic organoids compared to controls (Figure 2B-E, Supplemental Figure 3). Gene expression signatures of necroptosis and ferroptosis cell death pathways were also elevated in d20h organoids, which are known to have a pivotal role in the pathophysiology of AKI and progression to CKD (*48, 49*) (Figure 2B). Analysis of marker genes associated with the hypoxic response and kidney injury affirmed and extended our initial findings (Figure 2C). For example, injury and repair associated genes like *GDF15* (*50*), *TGFB1* (*51*), *JUN* (*52*), C-X-C motif chemokine ligand 1 (*CXCL1*) (*53*), snail family transcriptional repressor 1 (*SNAI1*) (*54*) and *SOX9* (*13, 55*) were higher in the d20h group compared to control (Figure 2C). Hypoxia can cause cell cycle arrest through the induction of cell cycle inhibitors like CDKN1A (*40, 56*). Increased expression of *CKDN1A* and decreased expression of the proliferation cell nuclear antigen (*PCNA*)

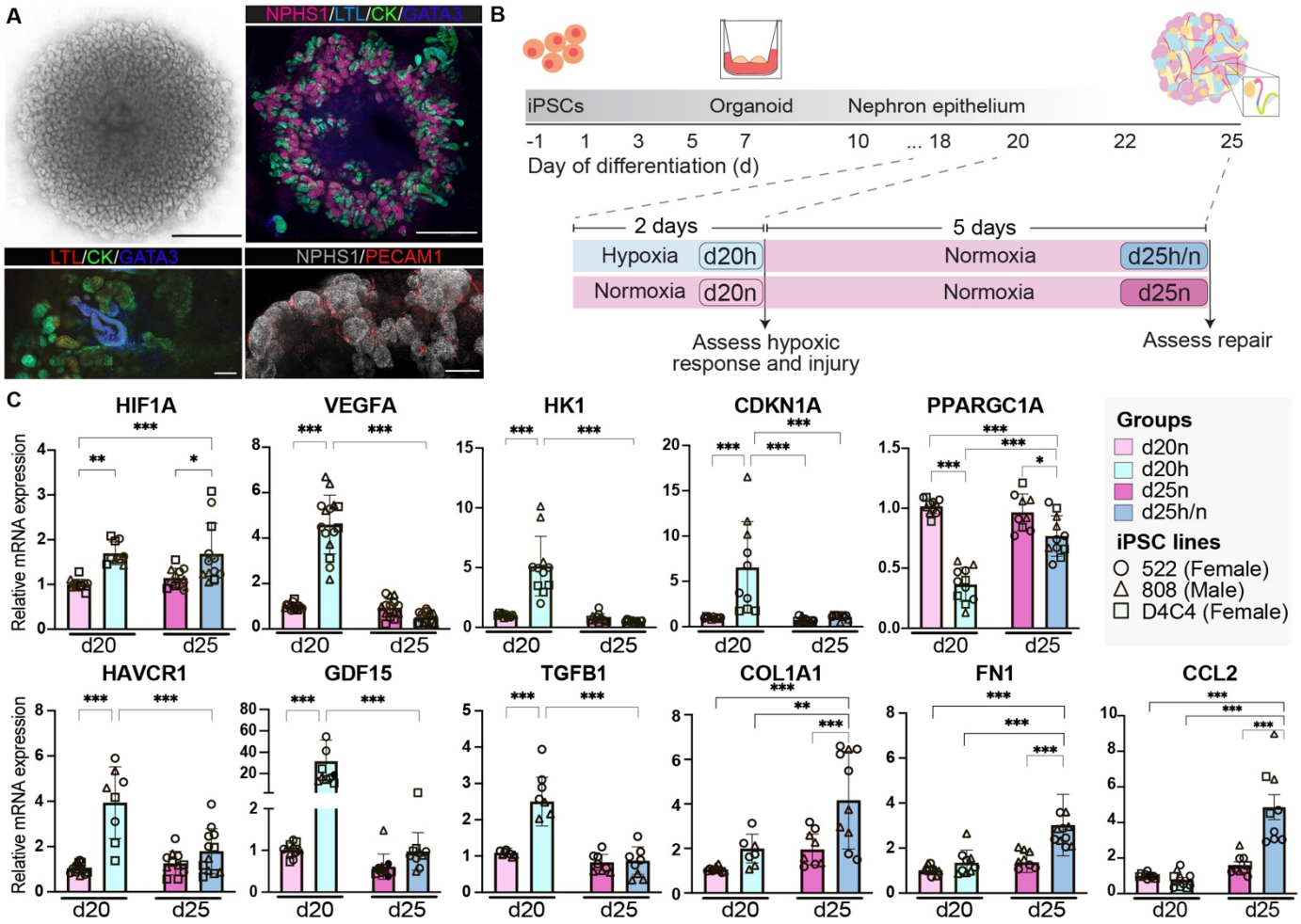

Figure 1. Evaluating hypoxic injury in kidney organoids from three iPSC lines. (A) Bright field and confocal images of day 18 kidney organoids labelled with markers of podocytes (NPHS1), tubular structures (CK), proximal tubule (LTL), distal tubule (GATA3) and endothelial cells (PECAM1). Scale bars: top images, 1000 µm; bottom images, 100 µm. **(B)** Overview of experiment illustrating differentiation and organoid generation from d-1 to d18, hypoxic exposure (d18-20), normoxic recovery (d20-d25), and sample collection points at d20 and d25. **(C)** qPCR analysis of hypoxic response genes (*HIF1A, VEGFA, HK1*), markers of cell cycle arrest (*CDKN1A*), mitochondrial function (*PPARGC1A*), kidney injury (*HAVCR1/KIM1, GDF15, TGFB1*), extracellular matrix (*COL1A1, FN1*) and inflammation (*CCL2*). Data shown as mean with SD; n=7-10. Y axis shows mRNA expression normalised to *ACTB* within each sample, relative to d20n mean. Analyses were performed by one-way ANOVA with Tukey's multiple comparison test: *p < 0.05, **p < 0.01, ***p < 0.001.

(*57*) were observed in d20h organoids (Figure 2C). These results were supported by gene set enrichment analysis (GSEA) showing decreased DNA replication, and enriched hypoxic response and p53 signatures associated with cell cycle arrest and apoptosis during AKI (*58*) (Figure 2D).

We have demonstrated that prophylactic JNK inhibition protects against ischemic AKI in rodents (*10, 59*). JNK activation is observed in most forms of human AKI (*52*) but JNK inhibition remains to be tested in the context of human kidney injury. With the increase in *JUN* mRNA and JNK-related p53 and apoptosis signatures in d20h organoids, we evaluated whether JNK inhibitor CC-401 protects against hypoxic injury in human kidney tissue. CC-401 or vehicle control were added an hour before culture in hypoxic or normoxic conditions, and a subset of markers were evaluated at d20. qPCR for *VEGFA* showed no effect of CC-401 or vehicle on the hypoxic response, while injury marker *GDF15* was significantly reduced by 5 and 10 µM CC-401.

JUN expression was also significantly reduced, consistent with an established autoregulatory role for this transcription factor (*52*). Expression of *CDKN1A* was highly variable but trended towards reduction in the CC-401-treated d20h organoids (Supplemental Figure 4). These results support a protective role for JNK inhibition in human AKI and illustrate the potential of human kidney organoids for drug screening.

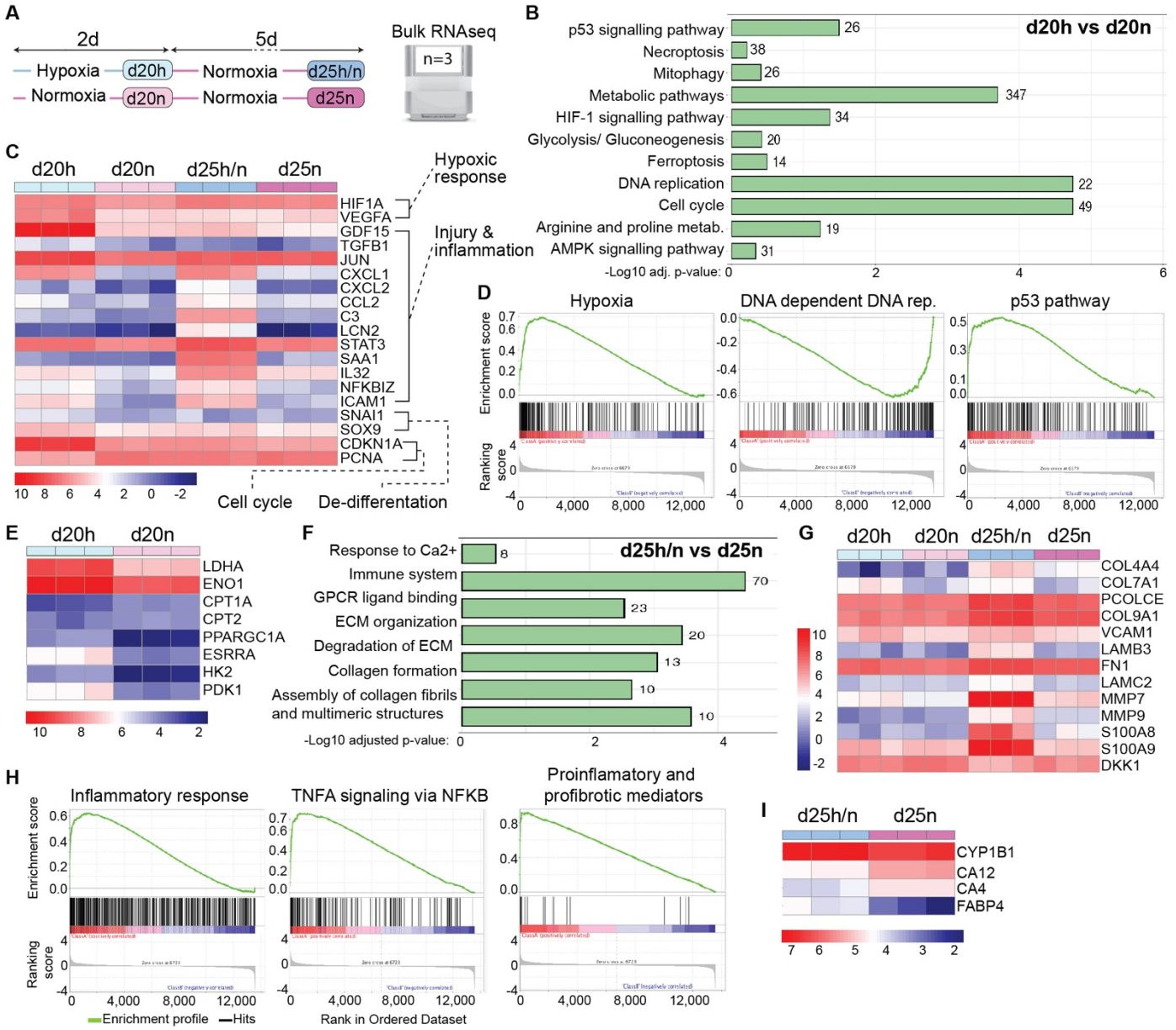

Figure 2. Transcriptional analysis of hypoxic injury and repair in kidney organoids. (A) Overview of bulk RNA-seq experiment. 3 replicates were generated from a pool of 2 organoids for each group. **(B)** Enrichment analysis highlights impacted pathways between d20h and d20n. Numbers of differentially expressed genes for each term are shown. **(C)** Heatmap of key genes related to hypoxic injury, inflammation, dedifferentiation and cell cycle, showing TMM normalized expression levels. **(D)** GSEA enrichment score density plots for select differentially regulated pathways between d20h and d20n. **(E)** Heatmap of key genes related to metabolism (*LDHA, ENO1, HK2, PDK1*) and mitochondrial function (*PPARGC1A, CPT1A/2, ESSRA*. (F) Enriched Biological Process terms between d25n and d25h/n. **(G)** Heatmap of key genes related to ECM and maladaptive repair. **(H)** Enrichment score density plots for select terms in d25n and d25h/n organoids. **(I)** Heatmap showing normalized expression levels of genes involved in metabolism and mitochondrial function in d25n and d25h/n organoids.

In physiological conditions, the balanced activities of glycolysis, the tricarboxylic acid (TCA) cycle, fatty acid oxidation, and oxidative phosphorylation (OXPHOS) maintain the energetic requirement of cells (*38*). During hypoxia, cells are forced to use oxygen-independent pathways like glycolysis to obtain adenosine triphosphate (ATP) at a lower efficiency (*38*). A shift towards glycolysis was evident in d20h organoids as reflected by increased expression of glycolytic enzymes such as lactate dehydrogenase-A (*LDHA*), hexokinase 2 (*HK2*), enolase1 (*ENO1*) and pyruvate dehydrogenase kinase 1 (*PDK1)* (*60*) (Figure 2E). Decreased expression of genes encoding mitochondrial enzymes and regulators carnitine palmitoyltransferase 1A and 2 (*CPT1* and *CPT2*), *PPARGC1A*, and the estrogen related receptor alpha (*ESRRA*) provide further evidence of mitochondrial dysfunction (Figure 2E).

We next compared the transcriptional profile of injured organoids at d25 (d25h/n) to controls (d25n) to investigate evidence of adaptive or maladaptive repair after recovery in normoxic conditions (Figure 2A, Supplemental Figure 5, Supplemental File 1). Extended culture of the iPSC-derived kidney organoid protocol we use (beyond day 25) has been linked to a decrease in organoid viability and stromal expansion (*21, 22, 31, 36*). Comparison of injured d25h/n organoids to stage-matched d25n controls revealed significant upregulation of pathways associated with ECM remodelling and maladaptive repair above and beyond changes over time in control organoids (Figure 2F). IRI studies in mice have identified a population of maladaptive PT characterized by a profibrotic and proinflammatory phenotype with upregulation of markers such as *S100a8 and S100a9* (*49*). These two markers increased by 13-fold increase in d25h/n organoids compared to d25n controls (Figure 2G). Despite the organoids lacking immune cells (*22*), differences in gene sets related to the immune system and inflammatory response were identified (Figure 2F, H). These signatures were based on increased expression of proinflammatory markers such as *CXCL1* (fold change (FC)=12)*, CXCL2* (FC=11), *ICAM1 (*FC=10)*,* complement component 3 (*C3,* FC=25)*,* signal transducer and activator of transcription 3 (*STAT3,* FC=2)*, CCL2* (FC=2)*,* lipocalin 2 (*LCN2,* also known as *NGAL*, FC=72) and interleukin 32 (*IL32,* FC=4) (*49, 61*) (Figure 2C). One of the top upregulated genes in d25h/n organoids was the serum amyloid A protein 1 (*SAA1*), which is regulated by STAT3 and known to contribute to inflammation and CKD progression (*62, 63*) (Figure 2C). SAA1 can induce endoplasmic reticulum stress favouring the development of interstitial fibrosis (*62*). Signatures associated with collagen formation and ECM remodelling were also enriched in d25h/n (Figure 2F-H). Marker genes associated with fibrosis including *COL7A1, COL4A4, PCOLCE, COL9A1, VCAM1, LAMB3, FN1, LAMC2,* and matrix metalloproteinases *MMP9* and *MMP7* were upregulated in d25h/n compared to d25n organoids (Figure 2G). Wnt inhibitor Dickkopf–related protein-1 *(DKK1)*, known to protect against fibrosis (*64, 65*), was downregulated in d25h/n organoids compared to d25n controls (Figure 2G). Dysregulation of fatty acid oxidation and bicarbonate metabolism have also been linked to CKD (*17, 66-68*). Increased expression of fatty acid-binding protein 4 (*FABP4*) and cytochrome P450 Family 1 Subfamily B Member 1, (*CYP1B1)* and decreased levels of carbonic anhydrase enzymes *CA12, CA4* were observed in d25h/n injured organoids, supporting further conservation of metabolic phenotypes associated with maladaptive repair (Figure 2I).

Maladaptive repair signatures after cisplatin treatment have been previously reported in kidney organoids (*26, 65*). Fanconi anemia complementation group D2 (*FANCD2*) and RAD51 recombinase (*RAD51*) were found to be downregulated in the cisplatin model of maladaptation (*26*). While we found expression of *FANCD2* and *RAD51* reduced immediately after hypoxia (d20), neither gene was significantly different in d25h/n organoids compared to d25n controls (Supplemental File 1). Although shared features of maladaptive repair are evident in both models, these results suggest distinct mechanisms of injury and repair following hypoxic and nephrotoxic insults.

Proteomic profiling affirms signatures of injury and maladaptive repair

To understand whether the transcriptional signatures of AKI and maladaptive repair were evident at the protein level, we performed untargeted LC-MS-based proteomics on 4 replicate samples from each experimental group (Figure 3A, Supplemental Figure 6). 844 proteins were found to differ significantly across the conditions out of a total of 3630 proteins quantified (Figure 3B, Supplemental File 2). Pathway enrichment analysis of differentially expressed proteins at d20 was consistent with the RNA-seq data; including HIF-1 signalling, metabolic and AMPK signalling pathways, among others (Supplemental Figure 6). GDF15 was found to be significantly increased during hypoxia by qPCR, bulk RNA-seq and proteomics (Figure 1C, 2C, 3C-D), and GDF15 protein remained elevated in the d25h/n organoid group (Figure 3E, Supplemental Figure 7). *GDF15* expression is elevated during ischemia and tubular damage in animal models and human kidney transplants (*50*), while circulating GDF15 levels correlate with increased risk of CKD progression (*69*). This aspect of AKI and maladaptation is conserved in our model. A

hypoxic response was evident by upregulation of hypoxic stress-responsive protein N-myc downstream-regulated gene 1 (NDRG1) (*70*), profibrotic HIF1 target CCN2 (*71*) and glycolytic enzymes HK1 and HK2 in d20h organoids (Figure 3C-D, Supplemental Figure 7). Hypoxia can reduce or arrest proliferation and impair lipid metabolism, signatures which were supported by decreased levels of PCNA (*57*) and phospholipid phosphatase 3 (PLPP3) (Figure 3C-D).

The organoid model used in this study does not contain immune cells (*21, 22*). However, stromal, endothelial and tubular epithelial cells within the kidney are known to respond to injury by expressing molecules involved in immune cell recruitment and activation. Increased levels of proinflammatory and profibrotic markers such as ICAM1, CXCL12, TGFB1 and STAT3 (*49, 61, 72*) were detected in d25h/n organoids compared to controls (Figure 3E-F, Supplemental Figure 7). Analysis of ICAM1 by immunofluorescence revealed that this protein is significantly increased in the tubular epithelium after injury (Figure 3G). The tubular injury marker HAVCR1 was not detected with MS-based proteomics, potentially due to low protein abundance, as supported by immunostaining (Supplemental Figure 8A). Single cell and spatial analysis of mouse ischemia-reperfusion injury models demonstrate that *Havcr1* expression peaks 6-12h after injury in segment 3 of the proximal tubule (*73, 74*). As such, the timepoints assayed in our study, the severity of injury, or the cellular composition of the organoids profiled may not reproduce this aspect of AKI. APOE, S100A8 and S100A9 proteins have been associated with maladaptive repair in the PT (*49, 75*) and were markedly increased in the d25h/n group (Figure 3H, Supplemental Figure 7). Increased expression of keratins KRT7, 8, 18 and 19 by injured tubules has been reported in both human and experimental models of kidney disease (*76, 77*). A significant increase in the levels of both KRT8 and KRT18 was identified in d25 injured organoids compared to all other groups (Figure 3E, Supplemental Figure 7).

Endoplasmic reticulum (ER) stress and the unfolded protein response (UPR) contribute to AKI and CKD progression, partly through excessive production of ROS (*78, 79*). Protein processing in the ER was identified as a differentially active pathway in both d20h vs d20n and d25h/n vs d25n comparisons (Supplemental Figure 6D), supported by increased levels of proteins such as UPR activator heat shock protein family A member 5 (HSPA5, also known as GRP78) in d20h and d25h/n, and ROS-scavenger mitochondrial protein superoxide dismutase 2 (SOD2) in d25h/n (Figure 3F, Supplemental Figure 7).

Tissue disorganization and nephron loss are pathological features of maladaptive kidney repair. Histological analysis of COL1 staining showed tissue disorganization and increased collagen deposition in d25h/n organoids compared to d25n controls (Figure 3I, Supplemental Figures 8B-C and 9). In contrast, the MS-based proteomic analysis did not detect a significant difference in the amount of collagen type I or type III (Supplemental Figure 7), which are also the most commonly found collagen types in fibrosis (*45*). However, the abundance of collagens including COL4A1, COL4A2, COL5A1 and COL6A1 was increased in d25 injured organoids, as was collagen triple helix repeat containing-1 (CTHRC1) which limits ECM deposition by reducing collagen type I mRNA and proteins (Supplemental Figure 7) (*80*). Cellular communication network factor 1 (CCN1) is induced in experimental models of AKI and contributes to the development of renal fibrosis (*81, 82*). CCN1 was among the most enriched proteins in the injury group at d20 and d25 (Figure 3C, E, Supplemental Figure 7).

Overall, the 844 differentially expressed proteins identified in this analysis represent a rich dataset of potential human biomarkers and consolidate findings based on gene expression. Moreover, the identification of emerging biomarkers like GDF15 and CCN1 highlight the potential of iPSC-derived human kidney organoids to validate markers of kidney injury observed in animal models.

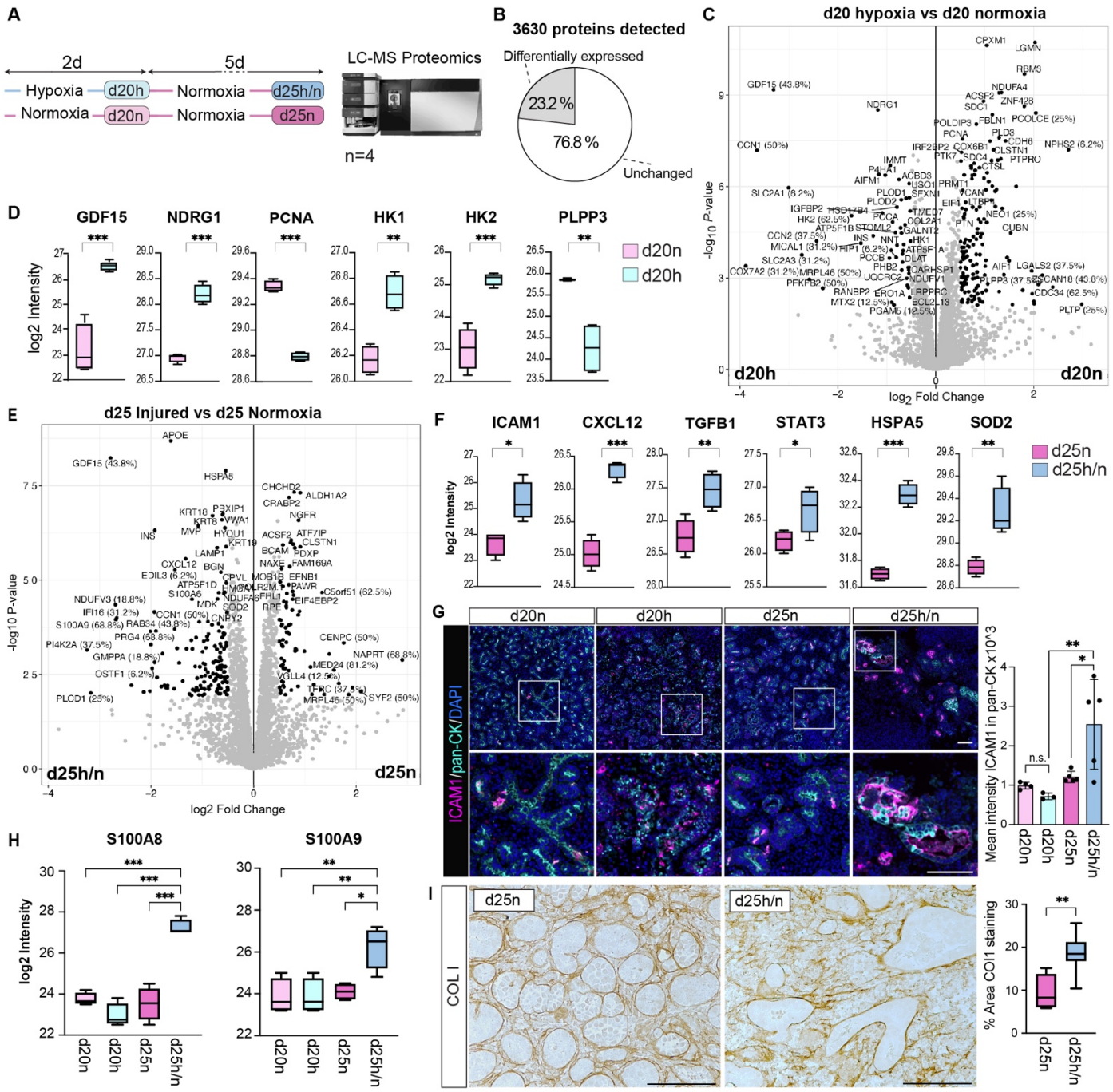

Figure 3. Proteomic analysis of hypoxic injury and repair. (**A**) Overview of MS-based proteomics indicating 4 replicates for each group. (**B**) Pie chart of differentially regulated proteins across all conditions. (**C**) Volcano plot of significantly changed proteins at d20. Percentage values indicate the extent of imputation during statistical analysis. (**D**) Intensity plots of proteins related to injury (GDF15), hypoxic response (NDRG1), cell cycle (PCNA) and metabolism (HK1, HK2, PLPP3) at d20. (**E**) Volcano plot of significantly changed proteins at d25. Percentage values indicate imputation. (**F**) Intensity plots of key proteins related to inflammatory and profibrotic processes (ICAM1, CXCL12, TGFB1, STAT3) and oxidative stress (HSPA5, SOD2) at d25. (**G**) Immunofluorescence for pan-cytokeratin (pan-CK, tubules), ICAM1 (inflammatory marker) and DAPI. Scale = 100 µm. Quantification of mean intensity of ICAM1 staining in tubules, n=4 replicates per experiment. n.s. non-significant, *$p < 0.05$, **$p < 0.01$. (**H**) Markers of maladaptive repair S100A8 and S100A9 are upregulated in d25h/n organoids. (**I**) Representative image of collagen type I (COL I) staining (n=4) showing tissue disorganization and increased COL I^+ area in d25h/n vs d25n. Scale bar = 500 µm. *$p < 0.05$, **$p < 0.01$, ***$p < 0.001$.

Single-cell RNA sequencing defines changes in the cellular composition of kidney organoids after hypoxic injury

We next used single-cell RNA-seq (scRNA-seq) to investigate changes in proliferation, cell proportions, AKI and maladaptive repair signatures. Three replicate sample pools from each experimental group were labelled with lipid-oligo barcodes and profiled on the 10x Chromium platform. Marker genes defined in the normoxic control samples were used as anchors to integrate the d20h and d25h/n samples, resulting in a combined dataset with over 12000 cells and 14 clusters at resolution 0.7 (Figure 4A-B, Supplemental Figure 10A, Supplemental File 3). Clusters with similarity to the early nephron, distal tubule, proximal tubule, podocytes, and endothelial cells were identified by expression of established marker genes (*83, 84*). Five stromal populations with similarity to renal cortical stroma, medullary stroma and mesangial cells were defined using a human kidney cell classifier (*85*). Gene set enrichment analysis was used to identify clusters defined by signatures of proliferation, cellular stress and off-target neural and myocyte-like populations (*86*) (Figure 4B-C).

The proportion of proximal tubule and endothelial cells recovered in this experiment was lower than expected. To assess whether this was an artefact of cell isolation or a general feature of the organoids in this study, we employed single cell deconvolution analysis (*87*) to assess organoid scRNAseq cluster signatures in our bulk RNAseq data. Higher proportions of proximal tubule and endothelial cell signatures were detected in the bulk RNAseq experiment, which was generated from a distinct batch of organoids (Supplemental Figure 10B). Thus the lower abundance of these cell types may be due to batch variation in the organoids (*20*), or cell dissociation artefacts, which can differentially affect the recovery of specific cell populations (*88*). Nonetheless, sufficient PT cells remained to examine signatures of injury and repair.

ScRNA-seq analysis of the proportion of cells per cluster between replicate samples and experimental groups was performed (*89*) (Figure 4D, Supplemental Figure 10C, Supplemental Tables 2-5). 'Proliferating' and endothelial clusters were reduced in d20 hypoxic organoids compared to d20n controls (false discovery rate, FDR<0.001 for both; Figure 4D). Increased proportions in the 'cellular stress' and stromal cluster 0 were observed in the d20h and d25h/n groups compared to stage-matched controls (FDR<0.01 for both). Stromal cluster 0 represented 18% of total cells in d25h/n organoids after recovery and only 8% in d25n controls. In contrast, stromal cluster 4 represented 7% of total cells in the injured d25h/n organoids compared to 14% of the cells profiled in d25 control organoids (FDR<0.01 for both). Thus, stromal cluster 0 expanded in response to hypoxic injury, while stromal cluster 4 increased over time in healthy controls. Fibrosis-associated genes like *SCRG1, SFRP2, KAZN* and *SCX* were identified as top markers for stromal cluster 0. In agreement with our histological findings of nephron loss, the proportion of combined nephron cell types (early nephron, proximal, distal, podocyte) was substantially reduced after hypoxic injury (30% d20h, 11% d25h/n) but remained stable in normoxic controls (20% d20n, 19% d25n) (Figure 4D). Notable changes within the nephron lineage include an apparent expansion in the distal nephron during hypoxia (14% d20h, 9% d20n FDR=0.02; Figure 4D),which may be explained by downregulation of segment-specific markers in the PT after hypoxic injury (*15*). Changes in early nephron and podocyte clusters is detailed in Supplemental Tables 2-5.

Cell cycle arrest in G1 (*90*) and G2/M (*91*) have been linked to AKI, while a proliferative response is associated with both adaptive and maladaptive repair. We investigated the proportion of cells with gene expression signatures correlating to G1, G2/M or S phase across experimental groups and within cell types in Seurat. Organoids cultured in hypoxic conditions had a dramatic increase in the proportion of cells in G1, paired with a decrease in S phase, suggestive of G1 arrest. A significant but smaller increase in G2/M was also observed in d20h and d25h/n organoids compared to controls (Figure 4E, Supplemental Figure 10D-E). At d25, injured organoids maintained a high proportion of G1 phase cells but mounted a proliferative response as evidenced by double the frequency of cells in S-phase cells in d25h/n compared to d25n controls. Cell cycle changes within nephron clusters mirrored findings from whole organoids (Figure 4E).

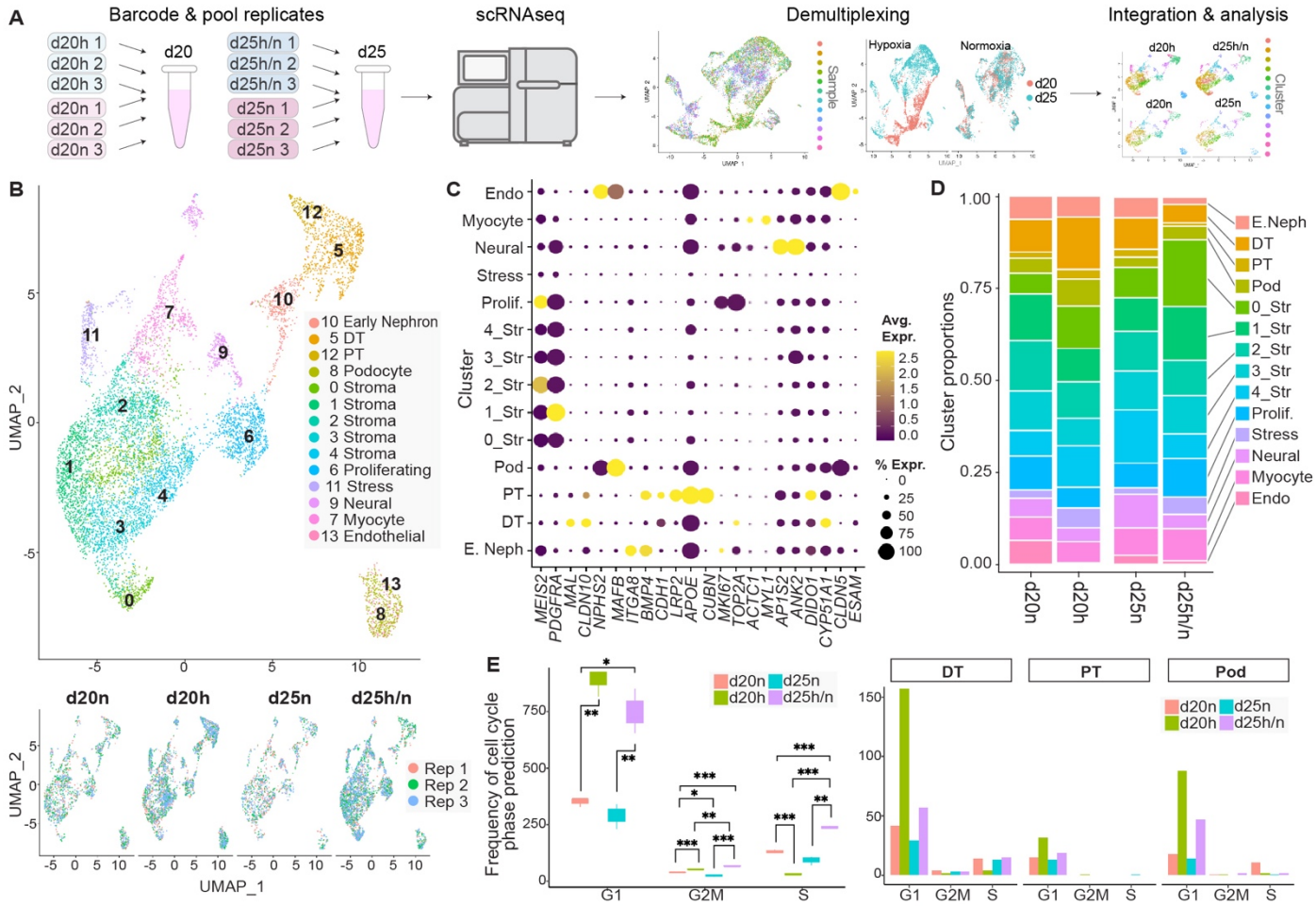

Figure 4. scRNAseq identifies changes in cell proportions and proliferation after hypoxic injury. (**A**) overview of scRNAseq experiment. (**B**) UMAP plot of integrated d20n, d20h, d25n and d25h/n organoid datasets coloured by cluster. Below, UMAP showing an even distribution of data from three replicates for each condition. (**C**) Dot plot of markers for each of the 14 clusters: stroma (*MEIS2, PDGFRA*), DT (*CLDN10, MAL*), podocytes (*NPHS2, MAFB*), early nephron (*ITGA8, BMP4*), PT (*LRP2, APOE, CUBN*), 'proliferating' (*MKI67, TOP2A*), 'cellular stress' (*DIDO1, CYP51A1*), muscle-like (*ACTC1, MYL1*) and neural (*AP1S2, ANK2*) and endothelial (*CLDN5, ESAM*). (**D**) Bar plot illustrating average proportions of clusters across replicates and conditions. (**E**) Box plot illustrating the frequency of cells in G1, G2/M and S phase of the cell cycle across all clusters (left), and within DT, PT and Pod clusters (right), *$p < 0.05$, **$p < 0.01$, ***$p < 0.001$.

Injury and maladaptive repair signatures are specific to the nephron lineage

We next performed differential expression analysis between injured and control groups in all scRNA-seq clusters to investigate the cellular basis of AKI and maladaptive repair signatures (Supplemental File 4, Supplemental Figure 11). All clusters responded to hypoxia with upregulation of *HIF1A* and *VEGFA*, and glycolysis markers *HK2, ENO1/2, GAPDH* and *LDHA* (Figure 5A). Expression of the cell cycle arrest marker CDKN1A was upregulated in PT, DT and podocytes of d20h organoids (adj. *p*-value<0.001), supporting our earlier results (Figure 5A-B). Transcriptional signatures of ferroptosis, autophagy, cell senescence, glycolysis/gluconeogenesis, and HIF1 pathways, VEGF, Hippo and AMPK signalling pathways were enriched in PT, DT and podocytes of d20 hypoxic organoids compared to controls (Supplemental Figure 11). Evidence of hypoxic injury in the nephron was supported by increased expression of *GDF15* and *CCN1* in PT, DT and podocyte clusters (Figure 5A-B). CCN1 is an early biomarker of kidney injury, which remains elevated in mouse unilateral ureteral obstruction models, suggesting a link to fibrotic progression (*81, 82*). *CCN1* expression was further increased in PT, DT and podocytes of d25 injured organoids (adj. *p*-value<0.001) (Figure 5B). Transcriptional signatures of TNF, NF-κB and JAK-STAT signalling pathways were also evident in PT, DT and podocyte clusters in d25 injured organoids (Supplemental

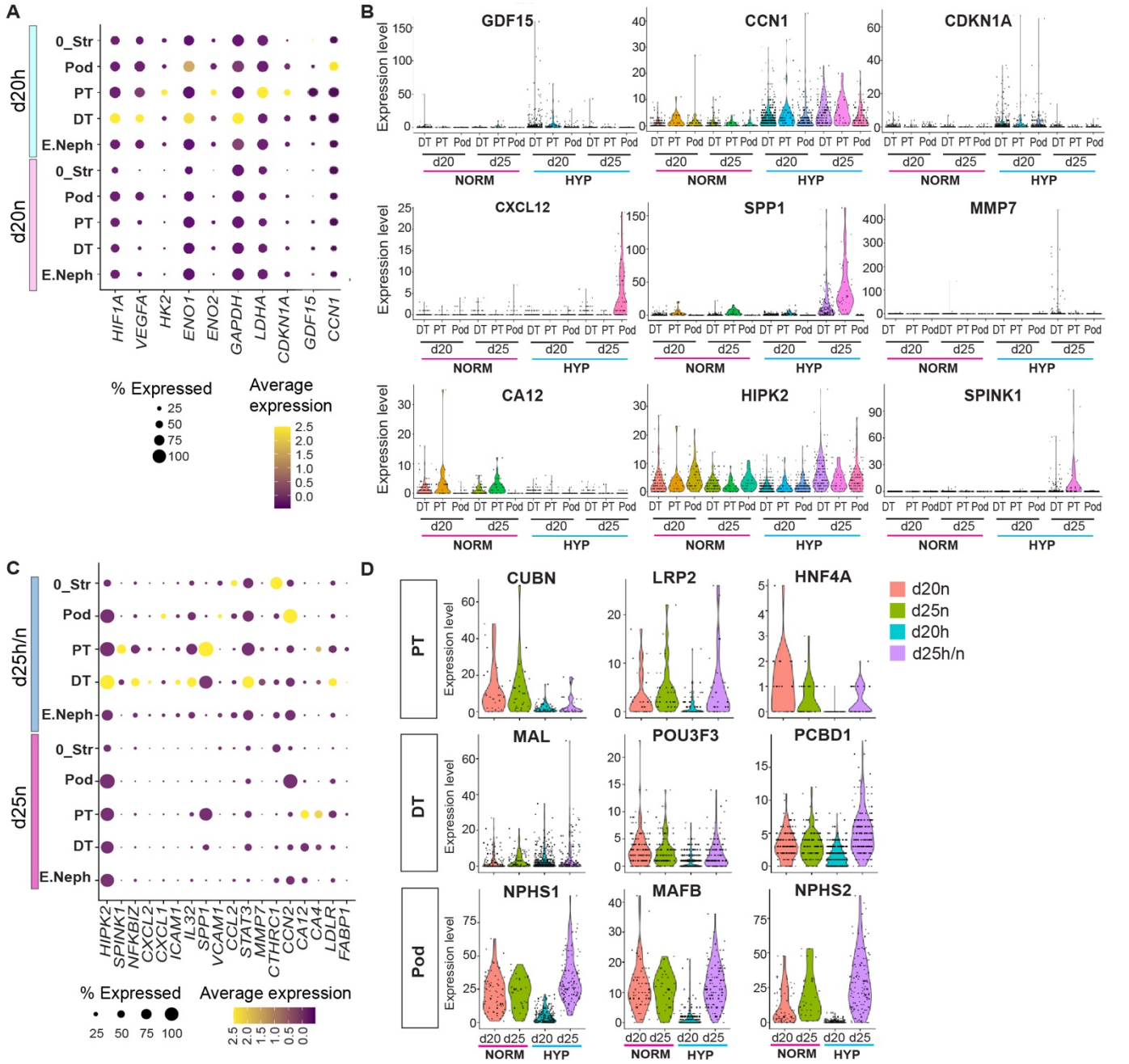

Figure 5. Proinflammatory and profibrotic signatures localise to tubular epithelial cells. (**A**) Dot plot of genes related to hypoxic injury across the different nephron clusters and a representative stromal cluster (cluster 0) at d20. (**B**) Violin plots of genes related to hypoxic injury across DT, PT and Pod clusters at d20 and d25. (**C**) Dot plot illustrating maladaptive repair markers across nephron clusters and a representative stromal cluster at d25. (**D**) Violin plots illustrating downregulation of segment-specific markers for PT, DT and podocytes in d20h and d25h/n groups.

Figure 11). HIPK2 has been identified as an activator of fibrosis in the kidney, which promotes oxidative stress, apoptosis and the induction of EMT markers in tubular cells (*14*). While expression of *HIPK2* was observed in all cell types, this gene was significantly upregulated in PT of d25h/n organoids (adj. *p*-value=0.02), as was SPINK1 (adj. *p*-value<0.001) - a senescence-associated secretory phenotype factor (*92*) (Figure 5B-C). Significantly increased expression of *NFKBIZ, CXCL2, ICAM1, IL32* and *SPP1* levels in DT, PT and podocyte clusters support a maladaptive repair phenotype, while low levels of *CA12* and *CA4* suggest impaired bicarbonate metabolism (Figure 5B-C). Podocytes from d25h/n organoids expressed high levels of *CXCL1, CXCL12* and *VCAM1* (Figure 5B-C). Cells of the injured stroma, in particular cluster 0, and podocytes produced higher levels of the monocyte chemoattractant CCL2; while MMP7 expression was increased in injured DT and PT clusters (adj. *p*-value<0.001) (Figure 5B-C). *CTHRC1*, which promotes remodelling, cell migration and inhibits collagen deposition

(*93*), was upregulated in stroma cluster 0, which was expanded after hypoxia (Figure 4C). CCN2 is implicated in the development of renal fibrosis after hypoxia (*71*) and was increased in both d20h and d25h/n organoid groups in the proteomic analysis. *CCN2* mRNA levels were significantly elevated in all stromal clusters (except cluster 4) and DT in d25h/n organoids compared to controls (adj. *p*-value<0.02) (Figure 5C, Supplemental File 4). However, small FC or non-significant *p*-values were found in podocyte (log FC=0.5; adj. *p*-value=0.02) and PT clusters (log FC=2; adj. *p*-value=0.07). Low-density lipoprotein receptor (LDLR) was found to be particularly increased in injured DT, while fatty acid-binding protein 1 (*FABP1*) was significantly increased in d25h/n PT (Figure 5C). *FABP1* is increased in AKI and CKD patients, and urinary FABP1 protein levels serve as a biomarker for AKI (*94*). Overall, we found expression of hypoxic response, injury and proinflammatory markers were highest in tubular epithelial cells, supporting increased susceptibility to hypoxia. Expression of cell type-specific markers was reduced within nephron clusters in response to hypoxic injury at d20, with some PT markers like *CUBN* and *HNF4A* remaining low in 25h/n organoids (Figure 5D).

These scRNA-seq data from hypoxic human kidney organoids identify a reduced proportion of nephron lineage cells, and expansion of a stromal sub population in response to hypoxic injury. AKI-related cell cycle signatures such as G1 arrest during early injury, and a proliferative response after injury were conserved. Importantly, these data localise injury and maladaptive repair signatures to the proximal and distal tubule and affirm the capacity of this human experimental model to validate and extend findings from animal and clinical studies of ischemic AKI.

Hypoxia drives metabolic dysregulation and mitochondrial dysfunction in kidney organoids

Our data suggest that hypoxia triggers immediate (d20) and longer term (d25) changes in mitochondrial function, energy production, lipid, amino acid and bicarbonate metabolism in human kidney organoids. To obtain a better understanding of these effects of hypoxia on human kidney organoids, we performed untargeted metabolomics using LC-MS using 8 replicates per experimental group (Figure 6A-B, Supplemental File 5). Metabolic profiles of replicate samples within each group were highly conserved, with substantial differences noted between d20h and d25h/n groups compared to controls (Figure 6B). Pathway enrichment analysis of metabolites detected in d20 hypoxic and d20 control organoids indicated dysregulation of arginine and proline metabolism, cysteine and methionine metabolism, the pentose phosphate pathway, TCA cycle, tryptophan metabolism, and glycolysis/gluconeogenesis (Figure 6C). Levels of ATP were decreased while lactate levels were increased in d20h organoids, consistent with a switch to glycolysis as a means of ATP synthesis in low oxygen conditions (Figure 6D). HIF-1 activity during prolonged hypoxia has been shown to decrease carbon flux into the TCA cycle (*95*), TCA-associated metabolites such as acetyl-CoA and oxalosuccinate were decreased in d20h organoids (Figure 6D). Hypoxia is thought to increase the biosynthesis of amino acids and favour pentose/hexose metabolism (*96*). Consistent with this, levels of tryptophan and serine, as well as putatively identified hexose-phosphate, were significantly increased in d20h organoids compared to d20n controls (Figure 6D). In addition, the levels of cellular antioxidant glutathione were significantly reduced (Figure 6D).

Metabolic dysregulation and mitochondrial dysfunction are associated with CKD (*17, 97*). Our gene and protein expression profiling data suggest changes in mitochondrial function, ATP, lipid and bicarbonate metabolism in d25h/n organoids. Enrichment analysis of metabolic profiles from d25h/n vs d25n organoids extended these findings, identifying several altered pathways including arginine and proline metabolism, glycerolipid and glycerophospholipid metabolism, steroid biosynthesis, sphingolipid metabolism, TCA cycle, tryptophan metabolism, and glycolysis/gluconeogenesis (Figure 6E). Dysregulated glycolipid metabolism was supported by Oil Red O staining in histological sections showing accumulation of neutral lipids, especially concentrated in tubular structures of d25h/n injured organoids (Figure 6F).

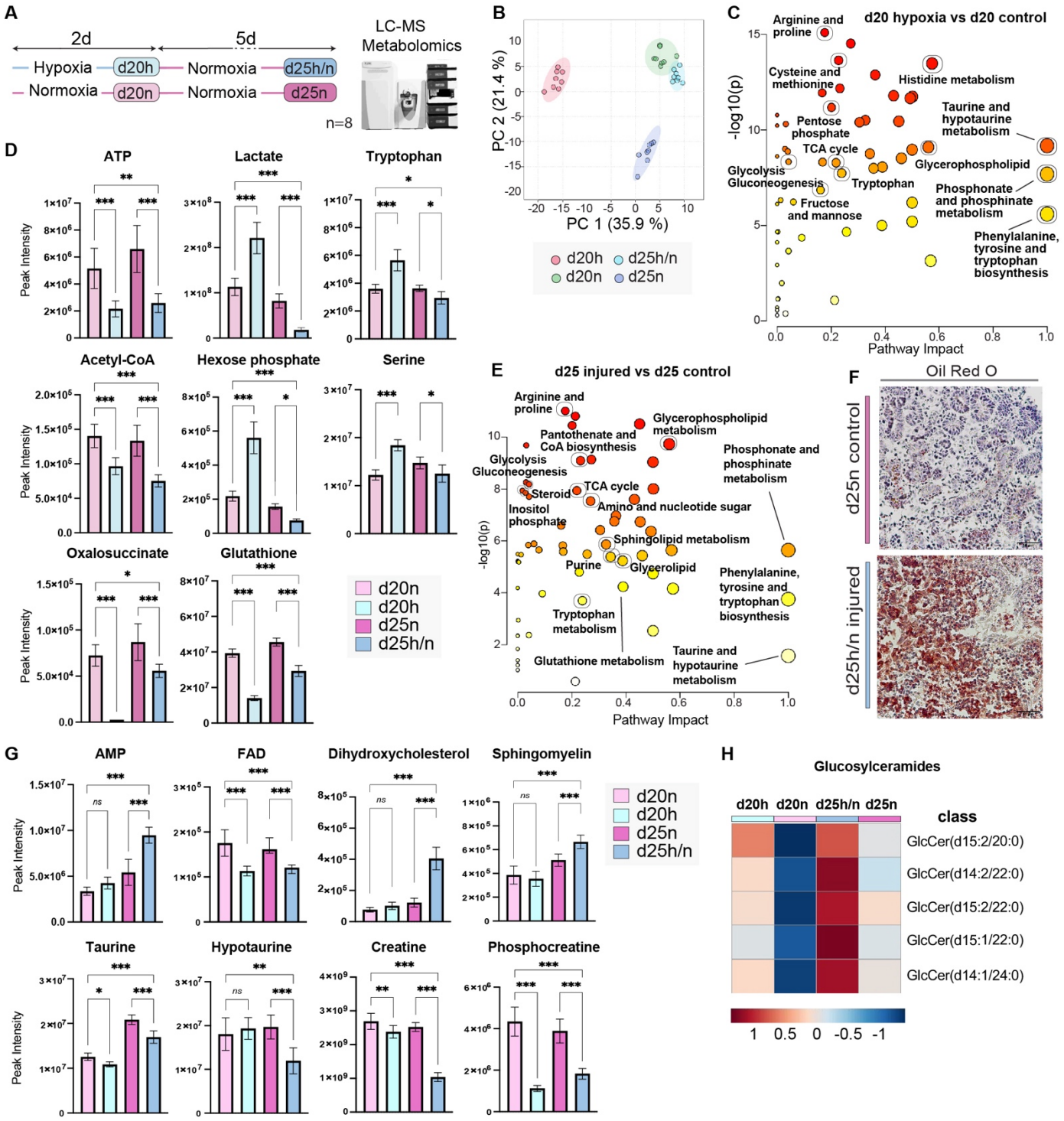

Figure 6. MS-based metabolomics supports metabolic dysregulation and mitochondrial disfunction during and after hypoxic injury. (**A**) Overview of metabolomic experiment with 8 replicates per condition. (**B**) PCA analysis of metabolomic data, which were normalized by the median, log10 transformed, and pareto scaled. (**C**) Metabolic pathway enrichment analysis to assess differences between d20h and d20n organoids. Circle size represents high pathway impact score (x-axis); y-axis indicates significance, with stronger *p*-values depicted in red. (**D**) Peak intensity of metabolites dysregulated after hypoxia. **p* < 0.05, ***p* < 0.01, ****p* < 0.001. (**E**) Pathway enrichment analysis between d25h and d25n organoids. (**F**) Oil Red O staining of control and injured organoids at d25. Scale bars = 50 µm. (**G**) Peak intensity of key metabolites that are associated with CKD and changed in d25 injured organoids. **p* < 0.05, ***p* < 0.01, ****p* < 0.001. (**H**) Heatmap showing five different glucosylceramide (GlcCer) species increased in d25h/n organoids.

Despite the 5-day recovery in normoxic conditions, d25h/n organoids failed to restore ATP to control levels. Instead, an increase of adenosine monophosphate (AMP) was observed (Figure 6G), resulting in a lower ATP/AMP ratio, which is indicative of energy shortage (*98*). Lower levels of TCA-associated metabolites oxalosuccinate, acetyl-Co-A and flavin adenine dinucleotide (FAD) were detected in d25h/n organoids (Figure 6D and 6G). This decrease in

TCA activity, even after restoration of normal oxygen levels, supports a maladaptive repair phenotype in d25h/n organoids involving substantial mitochondrial dysfunction.

Dyslipidaemia and lipotoxicity are known to contribute to CKD progression (*17*). Metabolites with similarity to dihydroxyxcholesterol, a type of oxysterol, were increased in d25 injured organoids (Figure 6G). Lipid peroxidation occurs during oxidative stress, dramatically increasing metabolites like oxysterols (*99*). Oxysterols are thought to mediate chronic inflammatory diseases and are increased in plasma of patients with chronic renal failure (*100*). Differences in sphingolipid metabolism were also evident in the metabolomic analysis. Increased levels of sphingomyelins and different classes of ceramides linked to kidney disease (*101*) were increased in d25 injured organoids (Figure 6G-H). This lipid accumulation could result from increased uptake, production, or reduced degradation. Increased lipid uptake is unlikely due to the absence of free fatty acids in the culture medium and low ATP levels in d25 injured organoids are expected to impair production. Therefore, the dyslipidaemia observed in d25h/n organoids is likely to result from reduced lipid degradation. Metabolic signatures associated with amino acid, purine and taurine metabolism were altered in d25h/n organoids, with taurine and hypotaurine significantly reduced in the d25h/n group (Figure 6G). A similar trend was found for other amino acids like tryptophan, creatine, and serine, which are found at reduced levels in the serum of patients with CKD (*97, 102-104*) (Figure 6G). Thus, human kidney organoids subjected to hypoxic injury recapitulate metabolic signatures associated with AKI and maladaptive repair.

DISCUSSION

Ischemia is a leading cause of AKI and an established driver of progression to renal failure in patients with existing CKD (*4*). Ischemic AKI has been extensively modelled in animals but investigations in a human context have largely been limited to analysis of biomarkers in the blood or urine, and study of renal epithelial cells in culture. There are no targeted therapies to suppress AKI or the transition to CKD, underscoring a need for scalable preclinical human models to interrogate disease mechanisms and test therapeutic strategies (*47*). In this study we employed transcriptional, proteomic and metabolic profiling to investigate how human kidney organoids respond to hypoxic injury. Our findings reveal a striking conservation of cellular processes, molecular biomarkers, signalling pathway activity, and metabolic characteristics associated with ischemic AKI and maladaptive repair from both animal models and clinical reports. Together with proof of principle data supporting a protective effect for JNK inhibitor CC-401, our results demonstrate the translational potential for kidney organoids as a human model of ischemic AKI and warrant further mechanistic and therapeutic studies.

Clinical biopsies are rarely taken from patients with AKI as diagnosis is based on serum creatinine levels and urine output and the biopsy procedure is often contraindicated. However, a recent atlas of healthy and injured cell states in the human kidney includes data from over 18 human AKI biopsies (*19*). These data link maladaptive repair to ageing, stress, senescence and inflammatory signatures, marked in part by elevated *CDKN1A* and *CCL2* expression and TGF-β, EGF, MAPK (FOS/JUN), NF-κB and JAK/STAT pathway signatures (*19*). Several of these features and pathways were identified in our study, providing an opportunity to test new mechanisms and hypotheses arising from clinical data in a human experimental model.

After affirming a robust hypoxic and injury response in organoids derived from three distinct induced pluripotent stem cell lines, we undertook a multiomic profiling approach to gain new insight into ischemic injury and maladaptive repair in humans. We identify conservation of AKI and maladaptive-associated cell cycle arrest, cell death, oxidative and ER stress, and inflammatory signatures in human kidney organoids. HIF1A-targets and genes associated with kidney injury like *GDF15*, *CCN1*, and *TGFB1* were upregulated in response to hypoxia. A maladaptive tubular repair phenotype was evident in injured organoids after a 5-day normoxic recovery by signatures of TNF, NF-κB and JAK-STAT pathway activation in the nephron epithelium, and expression of established markers of maladaptive tubular repair such as

ICAM1, S100A8 and *S100A9*. Elevated levels of GDF15 and CCN1 during hypoxic injury, and sustained CCN1 levels after injury demonstrates conservation of emerging biomarkers of early AKI and unresolved injury, and illustrate potential for further biomarker discovery and development in a human setting. Metabolic pathways involved in glycolysis and gluconeogenesis, amino acid metabolism, steroid hormone biosynthesis and lipid metabolism were dysregulated in d25h/n organoids. Metabolic dysregulation is a hallmark of CKD and an emerging area of interest in maladaptive repair. Thus, our model provides a unique opportunity to interrogate the role of metabolism in AKI and maladaptive repair without confounding syndromes or pre-existing disease. While species-specific differences are often cited as a reason for translational challenges, our study demonstrates broad conservation of injury and maladaptive repair signatures established in rodents and provides a scalable human experimental model in which to functionally evaluate their role.

Human kidney organoids have previously been used to model AKI resulting from nephrotoxins. Digby et al., found that a single high dose of cisplatin induced DNA damage and cell death, while a repeated low-dose regimen caused less toxicity while still inducing AKI biomarkers like *HAVCR1* and inflammatory cytokines (*65*). Using a similar repeated cisplatin exposure with a novel extended organoid culture protocol, Gupta et al., demonstrated that kidney organoids can model maladaptive repair and identified ineffective homology-directed DNA repair as the mechanism for this phenotype (*26*). In a model of hemolysis-induced AKI, Przepiorski et al., report induction of oxidative stress, *HAVCR1* and an early fibrotic phenotype marked by increased collagen production including COL1A1 (*25*). Our work modelling ischemic AKI shares induction of kidney injury markers, inflammatory signals, oxidative stress, early fibrosis and DNA damage with these studies. However, we also report differences like modest induction of *HAVCR1* despite upregulation of other injury markers like *GDF15, CCN1*, and *FABP1* in the PT. Ineffective DNA repair does not seem to be the major driver of maladaptive repair in our model. Instead, we link HIF1A, TNF, NF-κB and JAK-STAT signalling pathways and metabolic dysregulation with maladaptive repair after hypoxic injury. These findings are consistent with different mechanisms of repair in response to hypoxic and nephrotoxic insults and highlight the importance of modelling different drivers of kidney injury.

Despite the expression of profibrotic signals like TGFB1, CCN2 and MMP7, and expansion of a stromal population expressing relevant markers, fibrosis was not observed in this study. Documented limitations in the maturity of cell types within iPSC-derived kidney organoids and a lack of functional vasculature and immune cells apply (*32*). Future studies with alternative kidney organoid protocols enabling extended culture (*26*), enhanced maturation of specific cell types (*23, 24, 105*), or co-culture with macrophages (*106*) may improve the accuracy of this model. Further investigations will likely consider varying the levels and duration of oxygen exposure to more accurately represent physiological levels in the kidney (pO_2 of 50-10 mmHg cortex-medulla) (*107, 108*), and explore the spectrum of ischemic injury from mild hypoperfusion to complete cessation of blood flow. Despite these limitations, our results support a canonical HIF1A-mediated hypoxic response, and broad conservation of biomarkers and pathways associated with ischemic AKI and maladaptive repair.

Our study has identified conservation in the ischemic AKI response between organoids, adult patients and mature mouse models. However, cell types in iPSC-derived kidney organoids most closely reflect the human fetal kidney (*31*). As such, our model may also provide insight into how intrauterine hypoxia affects human kidney development. Epidemiological and animal studies link intrauterine hypoxia, low nephron number, and susceptibility to kidney disease in adulthood (*109*), but it remains unclear how and why human nephron formation is impaired. Our data illustrates that hypoxia induces loss of existing nephrons and altered nephron patterning in an invitro model of the human kidney. More importantly, progenitor cell populations responsible for ongoing nephron formation were depleted after hypoxic injury, providing a potential mechanistic link between intrauterine hypoxia and reduced nephron number.

We anticipate that our kidney organoid model of ischemic injury will enable mechanistic and screening studies *in vitro* to complement investigations in animal models and human patients. Indeed, we demonstrate that CC-401 protects against hypoxic injury for the first time in human kidney tissue and identify dysregulated pathways and metabolic processes as potential therapeutic targets. These activities illustrate the translational potential of human kidney organoids for ischemic AKI, which could hasten the development or repurposing of therapies to improve patient outcomes. Ischemia is a common cause of myocardial infarction and has pathological effects on multiple organ systems, including the brain. This study may be the most comprehensive characterisation of ischemic injury in any complex stem cell model and may serve as a reference for the study of ischemic injury in other human tissues and organs.

MATERIALS AND METHODS

Experimental Design

This study aimed to evaluate the capacity of iPSC-derived human kidney organoids to model hypoxic AKI and maladaptive repair. Select markers of AKI and maladaptive repair were assessed in multiple differentiations from three different iPSC lines to investigate reproducibility across different genetic backgrounds then a single iPSC line was used for transcriptional, proteomic, and metabolomic profiling. All experiments were performed using ≥3 biological replicates. Cell growth and organoid morphology was monitored by brightfield microscopy during each differentiation. iPSC cultures or batches of organoids that had slower rates of growth, unusual morphology, or poor nephron formation prior to d18 were discarded. Induction of hypoxic response and injury markers was confirmed by qPCR in each experimental batch. d18 kidney organoids were randomly assigned to experimental and control groups.

Hypoxic Injury

iPSC culture and kidney organoid generation (Takasato protocol) is detailed in supplementary materials. Hypoxic injury was modelled by culture in 1% O_2 for 48 h, repair was evaluated in injured organoids after a 5-day recovery in 19% O_2. Comparisons were made to stage-matched control organoids cultured in 19% O_2. Four organoids were cultured per transwell across all experiments to minimize potential variability in the diffusion and metabolism of nutrients and oxygen. For bulk RNA-sequencing, qPCR, proteomics and metabolomics studies, organoids were snap-frozen as soon as possible after removal from the incubator to preserve the biological state of interest.

Bulk and Single Cell RNAseq

For bulk RNAseq, total RNA was extracted from 3 individual replicate samples for each experimental group from a single differentiation. Sequencing was performed at the MHTP Medical Genomics facility using an established 3'-Multiplexed method. Further details on data processing, quality control and analysis are provided in the supplementary materials. Briefly, data were normalized using the CPM method and differentially expressed genes were defined using voom and limma R packages (*110, 111*), and Degust software (*112*) (BH adjusted p-value < 0.05 & absolute LogFC > 0.5). Enrichment analysis was performed with DAVID (*113*) and GSEA (*114*).

For Single cell RNA-seq, 3 iPSC-derived kidney organoids were pooled per replicate, with a total of 3 replicates per condition for d20n, d20h, d25h/n, d25n. Replicates were individually labelled with Cell Plex Cell Modified Oligonucleotides and processed on the day of collection. GEX and FB/CellPlex libraries were prepared using 10X Genomics Chromium Single Cell 5' V3.1 chemistry and sequenced on MGITech MGISEQ2000RS hardware using MGIEasy V3 chemistry for 100 bp paired-end sequencing. Quality control and analysis was performed using the R package Seurat (v. 4.3.0) (*115*) and related tools, see supplementary materials for details.

Untargeted Metabolomic and Proteomic Analysis

Eight individual replicate organoids per experimental group were harvested from a single differentiation. Proteins and metabolites were simultaneously extracted from each organoid. LC-MS based metabolomic data is typically more variable than an equivalent proteomic

dataset. As such, metabolites were profiled from all 8 samples in each experimental group while the proteome was profiled in only 4 samples per group. LC-MS proteomic analysis was conducted on an Orbitrap Fusion Tribrid mass spectrometer (Thermo Fisher Scientific) coupled to a Dionex Ultimate 3000 RSLCnano system. Raw data were analyzed with the Fragpipe software suite (*116*), and LFQ-Analyst was used for downstream statistical analysis (*117*). Significant changes in protein levels were defined in pairwise comparisons using adjusted p-value $\leq$ 0.05 (Benjamini-Hochberg method) and log2 fold change $\geq$ 0.5 or $\leq$ -0.5 thresholds. Untargeted metabolomic analysis was performed on a Dionex RSLC3000 UHPLC coupled to a Q-Exactive Plus MS (Thermo Fisher Scientific). Samples were analyzed by hydrophilic interaction liquid chromatography (HILIC) following a previously published method (*118*). Briefly, acquired LC-MS data were processed in an untargeted fashion using open source software IDEOM and related tools, which initially used msConvert (ProteoWizard)(*119*) to convert raw LC-MS files to mzXML format and XCMS to pick peaks to convert to .peakML files(*120*). Mzmatch was subsequently used for sample alignment and filtering (*121*). IDEOM was utilized for further data pre-processing, organization and quality evaluation (*120*). Full details on sample extraction and analysis are provided in supplementary materials.

Statistical Analysis

Details on sample number, statistical analyses and cutoff thresholds for each experiment included with the results and figures, or in methods and supplementary materials. All data points were included in the statistical analysis and displayed in related graphs where possible.

SUPPLEMENTAL MATERIALS

Supplemental Figures 1 to 11

Supplemental Tables 1 to 8

Supplemental Files 1 to 5

Acknowledgements: The authors acknowledge use of the MHTP Medical Genomics Facility, Micromon Genomics, Monash Histology Platform, Monash Bioinformatics Platform, and Monash Micro Imaging. This study used infrastructure enabled by Bioplatforms Australia and the National Collaborative Research Infrastructure Strategy at the Monash Proteomics and Metabolomics Platform. The authors would like to thank Rachel Lam for early contributions to the project. We thank Sara Howden and Melissa Little for support and providing the 522 and 808 iPSC lines, and Andrew Laslett for the D4C4 iPSC line.

Funding: The outlined work was supported in part by grants from the National Health and Medical Research Council of Australia grant APP1156567 (A.N.C.), the Medical Advances Without Animals Trust grant (A.N.C., A.B.N.-N., and D.J.N.-P.), and the Medical Research Future Fund APP2016033 (A.N.C.).

Author contributions: A.B.N.N, D.J.N.P. and A.N.C. conceived and designed the study; A.B.N.N administered the project, generated organoids, curated and interpreted data; M.P. performed and generated figures for the single cell deconvolution and bulk RNAseq analyses; L.P.J and D.D. curated and analysed the scRNAseq data; J.R.S. and H.L. prepared samples for proteomics, generated and analysed data; J.L.M performed and analysed the immunohistochemistry of ICAM and KIM1; C.K.B. undertook the untargeted metaboloics including sample preparation, LC-MS analysis and data analysis; R.B.S. provided resources, methodology and supervision for the MS study; Funding was acquired by A.N.C; The original draft was authored by A.B.N.N. and revised by A.N.C. with contributions from all authors; The project was supervised by D.J.N.P. and A.N.C; All authors reviewed and approved this manuscript.

Competing interests: No conflict of interest is declared by the authors.

Data and materials availability: All datasets related to this preprint will be made available on publication. The three iPSC lines in this study have been used under material transfer agreements with the Commonwealth Scientific and Industrial Research Organisation (CSIRO) and Murdoch Children's Research Institute (MCRI).

References

1. R. L. Mehta, J. Cerdá, E. A. Burdmann, M. Tonelli, G. García-García, V. Jha, P. Susantitaphong, M. Rocco, R. Vanholder, M. S. Sever, D. Cruz, B. Jaber, N. H. Lameire, R. Lombardi, A. Lewington, J. Feehally, F. Finkelstein, N. Levin, N. Pannu, B. Thomas, E. Aronoff-Spencer, G. Remuzzi, International Society of Nephrology's 0by25 initiative for acute kidney injury (zero preventable deaths by 2025): a human rights case for nephrology. *The Lancet* **385**, 2616-2643 (2015).
2. B. A. Molitoris, Low-Flow Acute Kidney Injury: The Pathophysiology of Prerenal Azotemia, Abdominal Compartment Syndrome, and Obstructive Uropathy. *Clinical Journal of the American Society of Nephrology* **17**, (2022).
3. J. B. O'Neal, A. D. Shaw, F. T. t. Billings, Acute kidney injury following cardiac surgery: current understanding and future directions. *Crit Care* **20**, 187 (2016).
4. J. V. Bonventre, L. Yang, Cellular pathophysiology of ischemic acute kidney injury. *J Clin Invest* **121**, 4210-4221 (2011).
5. P. Bhargava, R. G. Schnellmann, Mitochondrial energetics in the kidney. *Nat Rev Nephrol* **13**, 629-646 (2017).
6. S. Tanaka, T. Tanaka, M. Nangaku, Hypoxia and hypoxia-inducible factors in chronic kidney disease. *Renal Replacement Therapy* **2**, 25 (2016).
7. K. T. K. Giuliani, A. Grivei, P. Nag, X. Wang, M. Rist, K. Kildey, B. Law, M. S. Ng, R. Wilkinson, J. Ungerer, J. M. Forbes, H. Healy, A. J. Kassianos, Hypoxic human proximal tubular epithelial cells undergo ferroptosis and elicit an NLRP3 inflammasome response in CD1c(+) dendritic cells. *Cell Death Dis* **13**, 739 (2022).
8. A. Pefanis, F. L. Ierino, J. M. Murphy, P. J. Cowan, Regulated necrosis in kidney ischemia-reperfusion injury. *Kidney International* **96**, 291-301 (2019).
9. K. Grynberg, F. Y. Ma, D. J. Nikolic-Paterson, The JNK Signaling Pathway in Renal Fibrosis. *Front Physiol* **8**, 829 (2017).
10. K. Grynberg, E. Ozols, W. R. Mulley, R. J. Davis, R. A. Flavell, D. J. Nikolic-Paterson, F. Y. Ma, JUN Amino-Terminal Kinase 1 Signaling in the Proximal Tubule Causes Cell Death and Acute Renal Failure in Rat and Mouse Models of Renal Ischemia/Reperfusion Injury. *Am J Pathol* **191**, 817-828 (2021).
11. T. Kusaba, M. Lalli, R. Kramann, A. Kobayashi, B. D. Humphreys, Differentiated kidney epithelial cells repair injured proximal tubule. *Proceedings of the National Academy of Sciences* **111**, 1527-1532 (2014).
12. S. Kumar, J. Liu, P. Pang, A. M. Krautzberger, A. Reginensi, H. Akiyama, A. Schedl, Benjamin D. Humphreys, Andrew P. McMahon, Sox9 Activation Highlights a Cellular Pathway of Renal Repair in the Acutely Injured Mammalian Kidney. *Cell Reports* **12**, 1325-1338 (2015).
13. H. M. Kang, S. Huang, K. Reidy, S. H. Han, F. Chinga, K. Susztak, Sox9-Positive Progenitor Cells Play a Key Role in Renal Tubule Epithelial Regeneration in Mice. *Cell Rep* **14**, 861-871 (2016).
14. Y. Jin, K. Ratnam, P. Y. Chuang, Y. Fan, Y. Zhong, Y. Dai, A. R. Mazloom, E. Y. Chen, V. D'Agati, H. Xiong, M. J. Ross, N. Chen, A. Ma'ayan, J. C. He, A systems approach identifies HIPK2 as a key regulator of kidney fibrosis. *Nat Med* **18**, 580-588 (2012).
15. L. M. S. Gerhardt, K. Koppitch, J. van Gestel, J. Guo, S. Cho, H. Wu, Y. Kirita, B. D. Humphreys, A. P. McMahon, Lineage Tracing and Single-Nucleus Multiomics Reveal Novel Features of Adaptive and Maladaptive Repair after Acute Kidney Injury. *Journal of the American Society of Nephrology* **34**, (2023).
16. Z. Li, Z. Liu, M. Luo, X. Li, H. Chen, S. Gong, M. Zhang, Y. Zhang, H. Liu, X. Li, The pathological role of damaged organelles in renal tubular epithelial cells in the progression of acute kidney injury. *Cell Death Discovery* **8**, 239 (2022).
17. H. M. Kang, S. H. Ahn, P. Choi, Y.-A. Ko, S. H. Han, F. Chinga, A. S. D. Park, J. Tao, K. Sharma, J. Pullman, E. P. Bottinger, I. J. Goldberg, K. Susztak, Defective fatty acid oxidation in renal tubular epithelial cells has a key role in kidney fibrosis development. *Nature Medicine* **21**, 37-46 (2015).

18. M. Sugahara, S. Tanaka, T. Tanaka, H. Saito, Y. Ishimoto, T. Wakashima, M. Ueda, K. Fukui, A. Shimizu, R. Inagi, T. Yamauchi, T. Kadowaki, M. Nangaku, Prolyl Hydroxylase Domain Inhibitor Protects against Metabolic Disorders and Associated Kidney Disease in Obese Type 2 Diabetic Mice. *Journal of the American Society of Nephrology* **31**, (2020).
19. B. B. Lake, R. Menon, S. Winfree, Q. Hu, R. M. Ferreira, K. Kalhor, D. Barwinska, E. A. Otto, M. Ferkowicz, D. Diep, N. Plongthongkum, A. Knoten, S. Urata, L. H. Mariani, A. S. Naik, S. Eddy, B. Zhang, Y. Wu, D. Salamon, J. C. Williams, X. Wang, K. S. Balderrama, P. J. Hoover, E. Murray, J. L. Marshall, T. Noel, A. Vijayan, A. Hartman, F. Chen, S. S. Waikar, S. E. Rosas, F. P. Wilson, P. M. Palevsky, K. Kiryluk, J. R. Sedor, R. D. Toto, C. R. Parikh, E. H. Kim, R. Satija, A. Greka, E. Z. Macosko, P. V. Kharchenko, J. P. Gaut, J. B. Hodgin, M. T. Eadon, P. C. Dagher, T. M. El-Achkar, K. Zhang, M. Kretzler, S. Jain, An atlas of healthy and injured cell states and niches in the human kidney. *Nature* **619**, 585-594 (2023).
20. B. Phipson, P. X. Er, A. N. Combes, T. A. Forbes, S. E. Howden, L. Zappia, H. J. Yen, K. T. Lawlor, L. J. Hale, J. Sun, E. Wolvetang, M. Takasato, A. Oshlack, M. H. Little, Evaluation of variability in human kidney organoids. *Nat Methods* **16**, 79-87 (2019).
21. H. Wu, K. Uchimura, E. L. Donnelly, Y. Kirita, S. A. Morris, B. D. Humphreys, Comparative Analysis and Refinement of Human PSC-Derived Kidney Organoid Differentiation with Single-Cell Transcriptomics. *Cell Stem Cell* **23**, 869-881.e868 (2018).
22. A. N. Combes, L. Zappia, P. X. Er, A. Oshlack, M. H. Little, Single-cell analysis reveals congruence between kidney organoids and human fetal kidney. *Genome Medicine* **11**, 3 (2019).
23. A. B. Nunez-Nescolarde, D. J. Nikolic-Paterson, A. N. Combes, Human Kidney Organoids and Tubuloids as Models of Complex Kidney Disease. *The American Journal of Pathology*, (2022).
24. M. H. Little, A. N. Combes, Kidney organoids: accurate models or fortunate accidents. *Genes Dev* **33**, 1319-1345 (2019).
25. A. Przepiorski, T. Vanichapol, E. B. Espiritu, A. E. Crunk, E. Parasky, M. D. McDaniels, D. R. Emlet, R. Salisbury, C. L. Happ, L. A. Vernetti, M. L. MacDonald, J. A. Kellum, T. R. Kleyman, C. J. Baty, A. J. Davidson, N. A. Hukriede, Modeling oxidative injury response in human kidney organoids. *Stem Cell Res Ther* **13**, 76 (2022).
26. N. Gupta, T. Matsumoto, K. Hiratsuka, E. Garcia Saiz, P. Galichon, T. Miyoshi, K. Susa, N. Tatsumoto, M. Yamashita, R. Morizane, Modeling injury and repair in kidney organoids reveals that homologous recombination governs tubular intrinsic repair. *Sci Transl Med* **14**, eabj4772 (2022).
27. T. Ohmori, S. De, S. Tanigawa, K. Miike, M. Islam, M. Soga, T. Era, S. Shiona, K. Nakanishi, H. Nakazato, R. Nishinakamura, Impaired NEPHRIN localization in kidney organoids derived from nephrotic patient iPS cells. *Scientific Reports* **11**, 3982 (2021).
28. S. M. Czerniecki, N. M. Cruz, J. L. Harder, R. Menon, J. Annis, E. A. Otto, R. E. Gulieva, L. V. Islas, Y. K. Kim, L. M. Tran, T. J. Martins, J. W. Pippin, H. Fu, M. Kretzler, S. J. Shankland, J. Himmelfarb, R. T. Moon, N. Paragas, B. S. Freedman, High-Throughput Screening Enhances Kidney Organoid Differentiation from Human Pluripotent Stem Cells and Enables Automated Multidimensional Phenotyping. *Cell Stem Cell* **22**, 929-940.e924 (2018).
29. M. Lasse, J. El Saghir, C. C. Berthier, S. Eddy, M. Fischer, S. D. Laufer, D. Kylies, A. Hutzfeldt, L. L. Bonin, B. Dumoulin, R. Menon, V. Vega-Warner, F. Eichinger, F. Alakwaa, D. Fermin, A. M. Billing, A. Minakawa, P. J. McCown, M. P. Rose, B. Godfrey, E. Meister, T. Wiech, M. Noriega, M. Chrysopoulou, P. Brandts, W. Ju, L. Reinhard, E. Hoxha, F. Grahammer, M. T. Lindenmeyer, T. B. Huber, H. Schluter, S. Thiel, L. H. Mariani, V. G. Puelles, F. Braun, M. Kretzler, F. Demir, J. L. Harder, M. M. Rinschen, An integrated organoid omics map extends modeling potential of kidney disease. *Nat Commun* **14**, 4903 (2023).
30. S. E. Howden, M. H. Little, Generating Kidney Organoids from Human Pluripotent Stem Cells Using Defined Conditions. *Methods Mol Biol* **2155**, 183-192 (2020).

31. M. Takasato, P. X. Er, H. S. Chiu, B. Maier, G. J. Baillie, C. Ferguson, R. G. Parton, E. J. Wolvetang, M. S. Roost, S. M. Chuva de Sousa Lopes, M. H. Little, Kidney organoids from human iPS cells contain multiple lineages and model human nephrogenesis. *Nature* **526**, 564-568 (2015).
32. A. N. Combes, B. Phipson, K. T. Lawlor, A. Dorison, R. Patrick, L. Zappia, R. P. Harvey, A. Oshlack, M. H. Little, Single cell analysis of the developing mouse kidney provides deeper insight into marker gene expression and ligand-receptor crosstalk. *Development* **146**, dev178673 (2019).
33. X. Liang, D. M. Potenza, A. Brenna, Y. Ma, Z. Ren, X. Cheng, X. F. Ming, Z. Yang, Hypoxia Induces Renal Epithelial Injury and Activates Fibrotic Signaling Through Up-Regulation of Arginase-II. *Front Physiol* **12**, 773719 (2021).
34. B. S. Freedman, C. R. Brooks, A. Q. Lam, H. Fu, R. Morizane, V. Agrawal, A. F. Saad, M. K. Li, M. R. Hughes, R. V. Werff, D. T. Peters, J. Lu, A. Baccei, A. M. Siedlecki, M. T. Valerius, K. Musunuru, K. M. McNagny, T. I. Steinman, J. Zhou, P. H. Lerou, J. V. Bonventre, Modelling kidney disease with CRISPR-mutant kidney organoids derived from human pluripotent epiblast spheroids. *Nat Commun* **6**, 8715 (2015).
35. S. Tanigawa, E. Tanaka, K. Miike, T. Ohmori, D. Inoue, C.-L. Cai, A. Taguchi, A. Kobayashi, R. Nishinakamura, Generation of the organotypic kidney structure by integrating pluripotent stem cell-derived renal stroma. *Nature Communications* **13**, 611 (2022).
36. A. Przepiorski, V. Sander, T. Tran, J. A. Hollywood, B. Sorrenson, J. H. Shih, E. J. Wolvetang, A. P. McMahon, T. M. Holm, A. J. Davidson, A Simple Bioreactor-Based Method to Generate Kidney Organoids from Pluripotent Stem Cells. *Stem Cell Reports* **11**, 470-484 (2018).
37. R. Morizane, A. Q. Lam, B. S. Freedman, S. Kishi, M. T. Valerius, J. V. Bonventre, Nephron organoids derived from human pluripotent stem cells model kidney development and injury. *Nat Biotechnol* **33**, 1193-1200 (2015).
38. A. J. Majmundar, W. J. Wong, M. C. Simon, Hypoxia-Inducible Factors and the Response to Hypoxic Stress. *Molecular Cell* **40**, 294-309 (2010).
39. M. A. Venkatachalam, J. M. Weinberg, W. Kriz, A. K. Bidani, Failed Tubule Recovery, AKI-CKD Transition, and Kidney Disease Progression. *Journal of the American Society of Nephrology* **26**, 1765 (2015).
40. M. Koshiji, Y. Kageyama, E. A. Pete, I. Horikawa, J. C. Barrett, L. E. Huang, HIF-1alpha induces cell cycle arrest by functionally counteracting Myc. *Embo j* **23**, 1949-1956 (2004).
41. J.-W. Lee, S.-H. Bae, J.-W. Jeong, S.-H. Kim, K.-W. Kim, Hypoxia-inducible factor (HIF-1)α: its protein stability and biological functions. *Experimental & Molecular Medicine* **36**, 1-12 (2004).
42. M. Fontecha-Barriuso, D. Martin-Sanchez, J. M. Martinez-Moreno, M. Monsalve, A. M. Ramos, M. D. Sanchez-Niño, M. Ruiz-Ortega, A. Ortiz, A. B. Sanz, The Role of PGC-1α and Mitochondrial Biogenesis in Kidney Diseases. *Biomolecules*. 2020 (10.3390/biom10020347).
43. D. P. Basile, M. D. Anderson, T. A. Sutton, Pathophysiology of acute kidney injury. *Compr Physiol* **2**, 1303-1353 (2012).
44. R. A. Zager, A. C. M. Johnson, Acute kidney injury induces dramatic p21 upregulation via a novel, glucocorticoid-activated, pathway. *Am J Physiol Renal Physiol* **316**, F674-f681 (2019).
45. R. D. Bülow, P. Boor, Extracellular Matrix in Kidney Fibrosis: More Than Just a Scaffold. *Journal of Histochemistry & Cytochemistry* **67**, 643-661 (2019).
46. B. D. Humphreys, Mechanisms of Renal Fibrosis. *Annu Rev Physiol* **80**, 309-326 (2018).
47. D. A. Ferenbach, J. V. Bonventre, Mechanisms of maladaptive repair after AKI leading to accelerated kidney ageing and CKD. *Nat Rev Nephrol* **11**, 264-276 (2015).
48. A. Belavgeni, C. Meyer, J. Stumpf, C. Hugo, A. Linkermann, Ferroptosis and Necroptosis in the Kidney. *Cell Chem Biol* **27**, 448-462 (2020).
49. M. S. Balzer, T. Doke, Y. W. Yang, D. L. Aldridge, H. Hu, H. Mai, D. Mukhi, Z. Ma, R. Shrestha, M. B. Palmer, C. A. Hunter, K. Susztak, Single-cell analysis highlights

differences in druggable pathways underlying adaptive or fibrotic kidney regeneration. *Nat Commun* **13**, 4018 (2022).
50. J. Liu, S. Kumar, A. Heinzel, M. Gao, J. Guo, G. F. Alvarado, R. Reindl-Schwaighofer, A. M. Krautzberger, P. E. Cippà, J. McMahon, R. Oberbauer, A. P. McMahon, Renoprotective and Immunomodulatory Effects of GDF15 following AKI Invoked by Ischemia-Reperfusion Injury. *J Am Soc Nephrol* **31**, 701-715 (2020).
51. A. Sureshbabu, S. A. Muhsin, M. E. Choi, TGF-β signaling in the kidney: profibrotic and protective effects. *American Journal of Physiology-Renal Physiology* **310**, F596-F606 (2016).
52. K. Grynberg, F. Y. Ma, D. J. Nikolic-Paterson, The JNK Signaling Pathway in Renal Fibrosis. *Frontiers in Physiology* **8**, (2017).
53. H. Tang, M. Yang, Y. Liu, H. Liu, L. Sun, P. Song, The CXCL1-CXCR2 Axis Mediates Tubular Injury in Diabetic Nephropathy Through the Regulation of the Inflammatory Response. *Front Physiol* **12**, 782677 (2021).
54. R. Qi, J. Wang, Y. Jiang, Y. Qiu, M. Xu, R. Rong, T. Zhu, Snai1-induced partial epithelial-mesenchymal transition orchestrates p53-p21-mediated G2/M arrest in the progression of renal fibrosis via NF-κB-mediated inflammation. *Cell Death Dis* **12**, 44 (2021).
55. A. Prochnicki, K. Amann, M. Wegner, E. Sock, E. Pfister, S. Shankland, J. Pippin, C. Daniel, Characterization of Glomerular Sox9+ Cells in Anti-Glomerular Basement Membrane Nephritis in the Rat. *The American Journal of Pathology* **188**, 2529-2541 (2018).
56. B. Ortmann, J. Druker, S. Rocha, Cell cycle progression in response to oxygen levels. *Cell Mol Life Sci* **71**, 3569-3582 (2014).
57. Z. Saifudeen, J. Marks, H. Du, S. S. El-Dahr, Spatial repression of PCNA by p53 during kidney development. *American Journal of Physiology-Renal Physiology* **283**, F727-F733 (2002).
58. L. Liu, P. Zhang, M. Bai, L. He, L. Zhang, T. Liu, Z. Yang, M. Duan, M. Liu, B. Liu, R. Du, Q. Qian, S. Sun, p53 upregulated by HIF-1α promotes hypoxia-induced G2/M arrest and renal fibrosis in vitro and in vivo. *J Mol Cell Biol* **11**, 371-382 (2019).
59. J. Kanellis, F. Y. Ma, R. Kandane-Rathnayake, J. P. Dowling, K. R. Polkinghorne, B. L. Bennett, G. C. Friedman, D. J. Nikolic-Paterson, JNK signalling in human and experimental renal ischaemia/reperfusion injury. *Nephrology Dialysis Transplantation* **25**, 2898-2908 (2010).
60. X. Wang, X. Shen, Y. Yan, H. Li, Pyruvate dehydrogenase kinases (PDKs): an overview toward clinical applications. *Biosci Rep* **41**, (2021).
61. L. M. S. Gerhardt, J. Liu, K. Koppitch, P. E. Cippà, A. P. McMahon, Single-nuclear transcriptomics reveals diversity of proximal tubule cell states in a dynamic response to acute kidney injury. *Proceedings of the National Academy of Sciences* **118**, e2026684118 (2021).
62. F. Zhang, X. Zhou, H. Zou, L. Liu, X. Li, Y. Ruan, Y. Xie, M. Shi, Y. Xiao, Y. Wang, Y. Zhou, Y. Wu, B. Guo, SAA1 is transcriptionally activated by STAT3 and accelerates renal interstitial fibrosis by inducing endoplasmic reticulum stress. *Exp Cell Res* **408**, 112856 (2021).
63. R. J. Anderberg, R. L. Meek, K. L. Hudkins, S. K. Cooney, C. E. Alpers, R. C. Leboeuf, K. R. Tuttle, Serum amyloid A and inflammation in diabetic kidney disease and podocytes. *Lab Invest* **95**, 250-262 (2015).
64. B. G. Johnson, S. Ren, G. Karaca, I. G. Gomez, C. Fligny, B. Smith, A. Ergun, G. Locke, B. Gao, S. Hayes, S. MacDonnell, J. S. Duffield, Connective Tissue Growth Factor Domain 4 Amplifies Fibrotic Kidney Disease through Activation of LDL Receptor–Related Protein 6. *Journal of the American Society of Nephrology* **28**, 1769 (2017).
65. J. L. M. Digby, T. Vanichapol, A. Przepiorski, A. J. Davidson, V. Sander, Evaluation of cisplatin-induced injury in human kidney organoids. *American Journal of Physiology-Renal Physiology* **318**, F971-F978 (2020).
66. Y. Chen, Y. Dai, K. Song, Y. Huang, L. Zhang, C. Zhang, Q. Yan, H. Gao, Pre-emptive pharmacological inhibition of fatty acid–binding protein 4 attenuates kidney fibrosis by reprogramming tubular lipid metabolism. *Cell Death & Disease* **12**, 572 (2021).

67. K. Alka, J. R. Casey, Bicarbonate transport in health and disease. *IUBMB Life* **66**, 596-615 (2014).
68. B. L. Jennings, L. J. Anderson, A. M. Estes, F. A. Yaghini, X. R. Fang, J. Porter, F. J. Gonzalez, W. B. Campbell, K. U. Malik, Cytochrome P450 1B1 contributes to renal dysfunction and damage caused by angiotensin II in mice. *Hypertension* **59**, 348-354 (2012).
69. V. Nair, C. Robinson-Cohen, M. R. Smith, K. A. Bellovich, Z. Y. Bhat, M. Bobadilla, F. Brosius, I. H. de Boer, L. Essioux, I. Formentini, C. A. Gadegbeku, D. Gipson, J. Hawkins, J. Himmelfarb, B. Kestenbaum, M. Kretzler, M. C. Magnone, K. Perumal, S. Steigerwalt, W. Ju, N. Bansal, Growth Differentiation Factor-15 and Risk of CKD Progression. *J Am Soc Nephrol* **28**, 2233-2240 (2017).
70. H. Cangul, Hypoxia upregulates the expression of the NDRG1 gene leading to its overexpression in various human cancers. *BMC Genet* **5**, 27 (2004).
71. D. F. Higgins, M. P. Biju, Y. Akai, A. Wutz, R. S. Johnson, V. H. Haase, Hypoxic induction of Ctgf is directly mediated by Hif-1. *American Journal of Physiology-Renal Physiology* **287**, F1223-F1232 (2004).
72. D. Klimczak-Tomaniak, T. Pilecki, D. Żochowska, D. Sieńko, M. Janiszewski, L. Pączek, M. Kuch, CXCL12 in Patients with Chronic Kidney Disease and Healthy Controls: Relationships to Ambulatory 24-Hour Blood Pressure and Echocardiographic Measures. *Cardiorenal Med* **8**, 249-258 (2018).
73. E. E. Dixon, H. Wu, Y. Muto, P. C. Wilson, B. D. Humphreys, Spatially Resolved Transcriptomic Analysis of Acute Kidney Injury in a Female Murine Model. *J Am Soc Nephrol* **33**, 279-289 (2022).
74. H. Li, E. E. Dixon, H. Wu, B. D. Humphreys, Comprehensive single-cell transcriptional profiling defines shared and unique epithelial injury responses during kidney fibrosis. *Cell Metab* **34**, 1977-1998.e1979 (2022).
75. S. Ide, Y. Kobayashi, K. Ide, S. A. Strausser, K. Abe, S. Herbek, L. L. O'Brien, S. D. Crowley, L. Barisoni, A. Tata, P. R. Tata, T. Souma, Ferroptotic stress promotes the accumulation of pro-inflammatory proximal tubular cells in maladaptive renal repair. *eLife* **10**, e68603 (2021).
76. S. Djudjaj, M. Papasotiriou, R. D. Bülow, A. Wagnerova, M. T. Lindenmeyer, C. D. Cohen, P. Strnad, D. S. Goumenos, J. Floege, P. Boor, Keratins are novel markers of renal epithelial cell injury. *Kidney International* **89**, 792-808 (2016).
77. R. Moll, C. Hage, W. Thoenes, Expression of intermediate filament proteins in fetal and adult human kidney: modulations of intermediate filament patterns during development and in damaged tissue. *Lab Invest* **65**, 74-86 (1991).
78. C. A. Ricciardi, L. Gnudi, The endoplasmic reticulum stress and the unfolded protein response in kidney disease: Implications for vascular growth factors. *J Cell Mol Med* **24**, 12910-12919 (2020).
79. M. Yan, S. Shu, C. Guo, C. Tang, Z. Dong, Endoplasmic reticulum stress in ischemic and nephrotoxic acute kidney injury. *Ann Med* **50**, 381-390 (2018).
80. P. Pyagay, M. Heroult, Q. Wang, W. Lehnert, J. Belden, L. Liaw, R. E. Friesel, V. Lindner, Collagen triple helix repeat containing 1, a novel secreted protein in injured and diseased arteries, inhibits collagen expression and promotes cell migration. *Circ Res* **96**, 261-268 (2005).
81. Y. Muramatsu, M. Tsujie, Y. Kohda, B. Pham, A. O. Perantoni, H. Zhao, S. K. Jo, P. S. Yuen, L. Craig, X. Hu, R. A. Star, Early detection of cysteine rich protein 61 (CYR61, CCN1) in urine following renal ischemic reperfusion injury. *Kidney Int* **62**, 1601-1610 (2002).
82. C. F. Lai, Y. M. Chen, W. C. Chiang, S. L. Lin, M. L. Kuo, T. J. Tsai, Cysteine-rich protein 61 plays a proinflammatory role in obstructive kidney fibrosis. *PLoS One* **8**, e56481 (2013).
83. A. N. Combes, L. Zappia, P. X. Er, A. Oshlack, M. H. Little, Single-cell analysis reveals congruence between kidney organoids and human fetal kidney. *Genome Med* **11**, 3 (2019).
84. S. E. Howden, S. B. Wilson, E. Groenewegen, L. Starks, T. A. Forbes, K. S. Tan, J. M. Vanslambrouck, E. M. Holloway, Y. H. Chen, S. Jain, J. R. Spence, M. H. Little, Plasticity of

distal nephron epithelia from human kidney organoids enables the induction of ureteric tip and stalk. *Cell Stem Cell* **28**, 671-684.e676 (2021).
85. S. B. Wilson, S. E. Howden, J. M. Vanslambrouck, A. Dorison, J. Alquicira-Hernandez, J. E. Powell, M. H. Little, DevKidCC allows for robust classification and direct comparisons of kidney organoid datasets. *Genome Med* **14**, 19 (2022).
86. Z. Xie, A. Bailey, M. V. Kuleshov, D. J. B. Clarke, J. E. Evangelista, S. L. Jenkins, A. Lachmann, M. L. Wojciechowicz, E. Kropiwnicki, K. M. Jagodnik, M. Jeon, A. Ma'ayan, Gene Set Knowledge Discovery with Enrichr. *Curr Protoc* **1**, e90 (2021).
87. C. B. Steen, C. L. Liu, A. A. Alizadeh, A. M. Newman, Profiling Cell Type Abundance and Expression in Bulk Tissues with CIBERSORTx. *Methods Mol Biol* **2117**, 135-157 (2020).
88. E. Denisenko, B. B. Guo, M. Jones, R. Hou, L. de Kock, T. Lassmann, D. Poppe, O. Clément, R. K. Simmons, R. Lister, A. R. R. Forrest, Systematic assessment of tissue dissociation and storage biases in single-cell and single-nucleus RNA-seq workflows. *Genome Biol* **21**, 130 (2020).
89. B. Phipson, C. B. Sim, E. R. Porrello, A. W. Hewitt, J. Powell, A. Oshlack, propeller: testing for differences in cell type proportions in single cell data. *Bioinformatics* **38**, 4720-4726 (2022).
90. W.-g. Wang, W.-x. Sun, B.-s. Gao, X. Lian, H.-l. Zhou, Cell Cycle Arrest as a Therapeutic Target of Acute Kidney Injury. *Current Protein & Peptide Science* **18**, 1224-1231 (2017).
91. K. Taguchi, B. C. Elias, S. Sugahara, S. Sant, B. S. Freedman, S. S. Waikar, A. Pozzi, R. Zent, R. C. Harris, S. M. Parikh, C. R. Brooks, Cyclin G1 induces maladaptive proximal tubule cell dedifferentiation and renal fibrosis through CDK5 activation. *J Clin Invest* **132**, (2022).
92. F. Chen, Q. Long, D. Fu, D. Zhu, Y. Ji, L. Han, B. Zhang, Q. Xu, B. Liu, Y. Li, S. Wu, C. Yang, M. Qian, J. Xu, S. Liu, L. Cao, Y. E. Chin, E. W. F. Lam, J.-P. Coppé, Y. Sun, Targeting SPINK1 in the damaged tumour microenvironment alleviates therapeutic resistance. *Nature Communications* **9**, 4315 (2018).
93. D. Mei, Y. Zhu, L. Zhang, W. Wei, The Role of CTHRC1 in Regulation of Multiple Signaling and Tumor Progression and Metastasis. *Mediators of Inflammation* **2020**, 9578701 (2020).
94. E. Noiri, K. Doi, K. Negishi, T. Tanaka, Y. Hamasaki, T. Fujita, D. Portilla, T. Sugaya, Urinary fatty acid-binding protein 1: an early predictive biomarker of kidney injury. *Am J Physiol Renal Physiol* **296**, F669-679 (2009).
95. W. W. Wheaton, N. S. Chandel, Hypoxia. 2. Hypoxia regulates cellular metabolism. *Am J Physiol Cell Physiol* **300**, C385-393 (2011).
96. D. Rodriguez, D. Watts, D. Gaete, S. Sormendi, B. Wielockx, Hypoxia Pathway Proteins and Their Impact on the Blood Vasculature. *International Journal of Molecular Sciences*. 2021 (10.3390/ijms22179191).
97. D.-Q. Chen, G. Cao, H. Chen, C. P. Argyopoulos, H. Yu, W. Su, L. Chen, D. C. Samuels, S. Zhuang, G. P. Bayliss, S. Zhao, X.-Y. Yu, N. D. Vaziri, M. Wang, D. Liu, J.-R. Mao, S.-X. Ma, J. Zhao, Y. Zhang, Y.-Q. Shang, H. Kang, F. Ye, X.-H. Cheng, X.-R. Li, L. Zhang, M.-X. Meng, Y. Guo, Y.-Y. Zhao, Identification of serum metabolites associating with chronic kidney disease progression and anti-fibrotic effect of 5-methoxytryptophan. *Nature Communications* **10**, 1476 (2019).
98. D. G. Hardie, Minireview: The AMP-Activated Protein Kinase Cascade: The Key Sensor of Cellular Energy Status. *Endocrinology* **144**, 5179-5183 (2003).
99. N. Florens, C. Calzada, E. Lyasko, L. Juillard, C. O. Soulage, Modified Lipids and Lipoproteins in Chronic Kidney Disease: A New Class of Uremic Toxins. *Toxins (Basel)* **8**, (2016).
100. W. Siems, S. Quast, D. Peter, W. Augustin, F. Carluccio, T. Grune, A. Sevanian, H. Hampl, I. Wiswedel, Oxysterols are increased in plasma of end-stage renal disease patients. *Kidney Blood Press Res* **28**, 302-306 (2005).
101. R. J. Nicholson, M. G. Pezzolesi, S. A. Summers, Rotten to the Cortex: Ceramide-Mediated Lipotoxicity in Diabetic Kidney Disease. *Front Endocrinol (Lausanne)* **11**, 622692 (2020).

102. Y. Cheng, Y. Li, P. Benkowitz, C. Lamina, A. Köttgen, P. Sekula, The relationship between blood metabolites of the tryptophan pathway and kidney function: a bidirectional Mendelian randomization analysis. *Scientific Reports* **10**, 12675 (2020).
103. J. H. Salazar, Overview of Urea and Creatinine. *Laboratory Medicine* **45**, e19-e20 (2014).
104. A. Post, D. Tsikas, S. J. L. Bakker, Creatine is a Conditionally Essential Nutrient in Chronic Kidney Disease: A Hypothesis and Narrative Literature Review. *Nutrients* **11**, (2019).
105. J. M. Vanslambrouck, S. B. Wilson, K. S. Tan, E. Groenewegen, R. Rudraraju, J. Neil, K. T. Lawlor, S. Mah, M. Scurr, S. E. Howden, K. Subbarao, M. H. Little, Enhanced metanephric specification to functional proximal tubule enables toxicity screening and infectious disease modelling in kidney organoids. *Nature Communications* **13**, 5943 (2022).
106. K. T. Kroll, M. M. Mata, K. A. Homan, V. Micallef, A. Carpy, K. Hiratsuka, R. Morizane, A. Moisan, M. Gubler, A. C. Walz, E. Marrer-Berger, J. A. Lewis, Immune-infiltrated kidney organoid-on-chip model for assessing T cell bispecific antibodies. *Proc Natl Acad Sci U S A* **120**, e2305322120 (2023).
107. M. Brezis, S. N. Heyman, F. H. Epstein, Determinants of intrarenal oxygenation. II. Hemodynamic effects. *American Journal of Physiology-Renal Physiology* **267**, F1063-F1068 (1994).
108. P. Liss, A. Nygren, N. P. Revsbech, H. R. Ulfendahl, Intrarenal oxygen tension measured by a modified clark electrode at normal and low blood pressure and after injection of x-ray contrast media. *Pflugers Arch* **434**, 705-711 (1997).
109. V. A. Luyckx, B. M. Brenner, Clinical consequences of developmental programming of low nephron number. *Anat Rec (Hoboken)* **303**, 2613-2631 (2020).
110. M. E. Ritchie, B. Phipson, D. Wu, Y. Hu, C. W. Law, W. Shi, G. K. Smyth, limma powers differential expression analyses for RNA-sequencing and microarray studies. *Nucleic acids research* **43**, e47-e47 (2015).
111. C. W. Law, Y. Chen, W. Shi, G. K. Smyth, voom: Precision weights unlock linear model analysis tools for RNA-seq read counts. *Genome biology* **15**, 1-17 (2014).
112. D. Powell, Degust: interactive RNA-seq analysis. *Drpowell/Degust* **4**, 4.1 (2015).
113. B. T. Sherman, M. Hao, J. Qiu, X. Jiao, M. W. Baseler, H. C. Lane, T. Imamichi, W. Chang, DAVID: a web server for functional enrichment analysis and functional annotation of gene lists (2021 update). *Nucleic acids research* **50**, W216-W221 (2022).
114. A. Subramanian, P. Tamayo, V. K. Mootha, S. Mukherjee, B. L. Ebert, M. A. Gillette, A. Paulovich, S. L. Pomeroy, T. R. Golub, E. S. Lander, Gene set enrichment analysis: a knowledge-based approach for interpreting genome-wide expression profiles. *Proceedings of the National Academy of Sciences* **102**, 15545-15550 (2005).
115. Y. Hao, S. Hao, E. Andersen-Nissen, W. M. Mauck, 3rd, S. Zheng, A. Butler, M. J. Lee, A. J. Wilk, C. Darby, M. Zager, P. Hoffman, M. Stoeckius, E. Papalexi, E. P. Mimitou, J. Jain, A. Srivastava, T. Stuart, L. M. Fleming, B. Yeung, A. J. Rogers, J. M. McElrath, C. A. Blish, R. Gottardo, P. Smibert, R. Satija, Integrated analysis of multimodal single-cell data. *Cell* **184**, 3573-3587 e3529 (2021).
116. G. C. Teo, D. A. Polasky, F. Yu, A. I. Nesvizhskii, Fast Deisotoping Algorithm and Its Implementation in the MSFragger Search Engine. *J Proteome Res* **20**, 498-505 (2021).
117. A. D. Shah, R. J. A. Goode, C. Huang, D. R. Powell, R. B. Schittenhelm, LFQ-Analyst: An Easy-To-Use Interactive Web Platform To Analyze and Visualize Label-Free Proteomics Data Preprocessed with MaxQuant. *Journal of Proteome Research* **19**, 204-211 (2020).
118. D. Stoessel, C. Nowell, A. Jones, L. Ferrins, K. Ellis, J. Riley, R. Rahmani, K. Read, M. McConville, V. Avery, Metabolomics and lipidomics reveal perturbation of sphingolipid metabolism by a novel anti-trypanosomal 3-(oxazolo [4, 5-b] pyridine-2-yl) anilide. *Metabolomics* **12**, 126 (2016).
119. M. C. Chambers, B. Maclean, R. Burke, D. Amodei, D. L. Ruderman, S. Neumann, L. Gatto, B. Fischer, B. Pratt, J. Egertson, K. Hoff, D. Kessner, N. Tasman, N. Shulman, B. Frewen, T. A. Baker, M.-Y. Brusniak, C. Paulse, D. Creasy, L. Flashner, K. Kani, C.

Moulding, S. L. Seymour, L. M. Nuwaysir, B. Lefebvre, F. Kuhlmann, J. Roark, P. Rainer, S. Detlev, T. Hemenway, A. Huhmer, J. Langridge, B. Connolly, T. Chadick, K. Holly, J. Eckels, E. W. Deutsch, R. L. Moritz, J. E. Katz, D. B. Agus, M. MacCoss, D. L. Tabb, P. Mallick, A cross-platform toolkit for mass spectrometry and proteomics. *Nature Biotechnology* **30**, 918-920 (2012).

120. D. J. Creek, A. Jankevics, K. E. Burgess, R. Breitling, M. P. Barrett, IDEOM: an Excel interface for analysis of LC-MS-based metabolomics data. *Bioinformatics* **28**, 1048-1049 (2012).

121. R. A. Scheltema, A. Jankevics, R. C. Jansen, M. A. Swertz, R. Breitling, PeakML/mzMatch: a file format, Java library, R library, and tool-chain for mass spectrometry data analysis. *Anal Chem* **83**, 2786-2793 (2011).